UCID- 17576

Lawrence Livermore Laboratory

REVIEW OF ELECTROSTATIC PLUGGING

T. J. Dolan

August 10, 1977

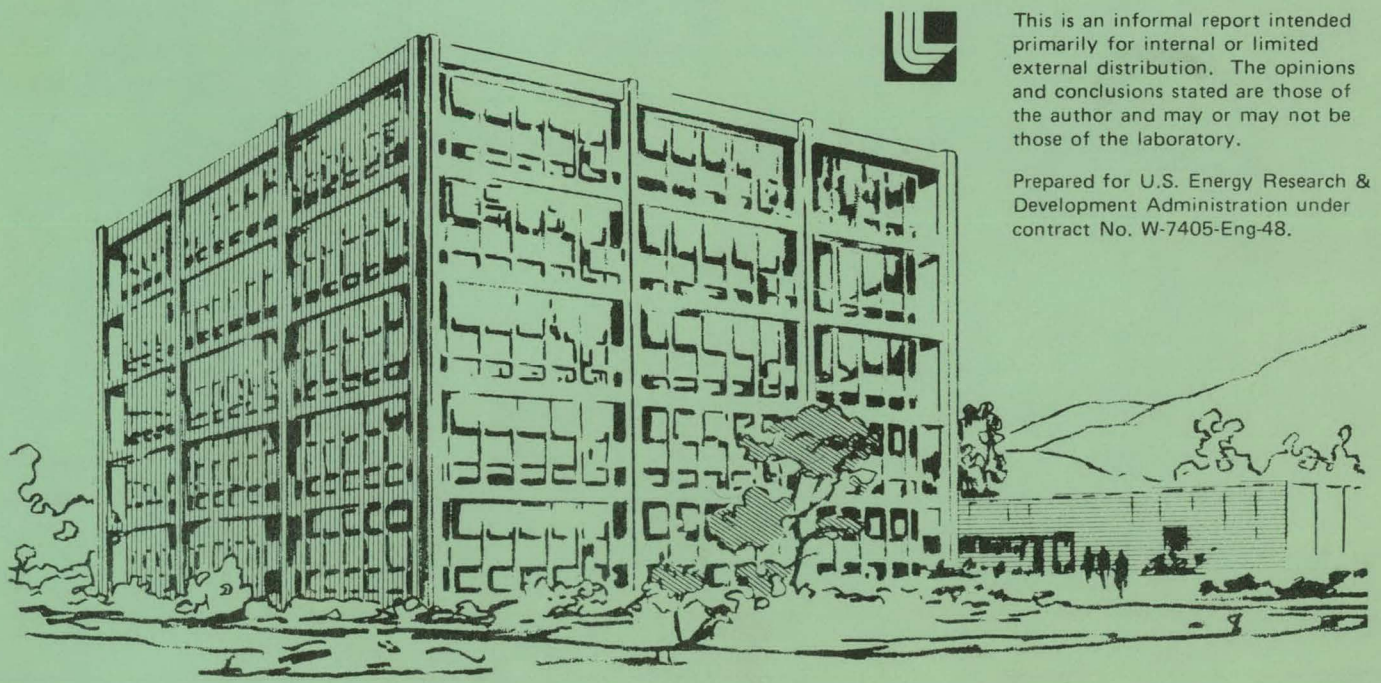

Prepared for U.S. Energy Research & Development Administration under contract No. W-7405-Eng-48.

DISCLAIMER

REVIEW OF ELECTROSTATIC PLUGGING*

T. J. Dolan**
Lawrence Livermore Laboratory,
University of California
Livermore, California 94550

ABSTRACT

Using electric fields to diminish end losses from open magnetic plasma confinement systems is equivalent to magnetically shielding the grid wires of an electrostatic plasma confinement device. Electrostatically plugged magnetic cusps confine electrons magnetically in the perpendicular direction and electrostatically in the parallel direction, and ions are purely electrostatically confined in both directions. Theoretical estimates have been made of confinement times, electron density, plasma potential, and plasma temperatures. Experimentally, plasmas with $n = 5 \times 10^{12}$ cm^{-3}, $T_i = 1$ keV, $\tau = 5$ msec, have been confined by cusp fields of about 10 kG with applied voltages $\sim$ 10 kV. Fusion reactors with (fusion power)/(injection power) $\equiv Q \sim 5$ appear feasible using $B \sim 80$ kG, applied voltage $\sim$ 300 kV, if extrapolations from present experiments hold. Electrostatically plugged cusps are similar in some ways to Tandem Mirrors, to Tormac, and to SURMAC plasma confinement systems.

---

*Work performed under the auspices of the U.S. Energy Research & Development Administration under contract No. W-7405-Eng-48.

**University of Missouri, Rolla

TABLE OF CONTENTS

BACKGROUND

Electrostatic plasma confinement was proposed in the 1950's by Farnsworth and by Wells in the USA, and by Lavrent'ev in the USSR.[1,2] Early electrostatic plasma confinement experiments consist of concentric spherical wire mesh electrodes which accelerated charged particles inwards to produce a virtual electrode inside the central sphere (Fig. 1). For example, if electrons were injected into the sphere, they would produce a virtual cathode, which could trap energetic ions. For the case of electron injection, it appeared that there are two difficulties: prohibitively high currents would be required for a reactor,[2] and grid wires would melt. Calculations of grid wire heating from charged particle bombardment and cooling by radiation indicated that better $n\tau$ values could be obtained for the case of a pulsed reactor, and for the case of ion injection, but that the Lawson criterion could probably not be attained with a reasonable device radius.[3] At the same time, high neutron yields were observed from a steady-state device using ion injection from six ion guns;[4] these neutron yields exceeded the predictions of simple theories. One hypothesis which could account for the observed neutron yields is the formation of multiple, concentric, spherical potential wells of alternate sign inside the central sphere, with circulating currents higher in the inside layers, as illustrated in Fig. 2. According to such a model, ions trapped in interior layers could have high energies and densities, producing significant fusion energy yields. Recent theoretical and experimental studies indicate that two or more concentric spherical potential wells may

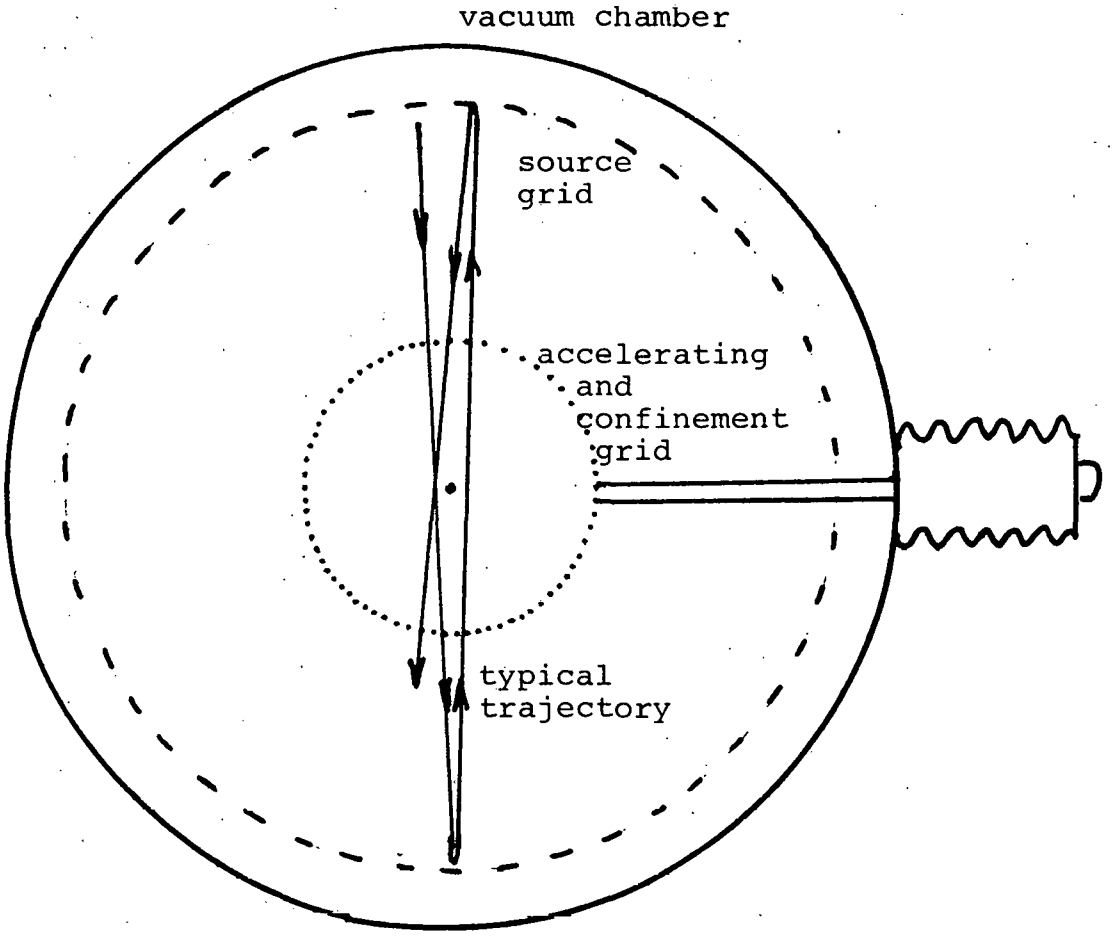

Fig. 1. Schematic diagram of electrostatic-inertial plasma confinement. Charged particles emitted by the source grid are accelerated inwards through the central grid. A dense, hot plasma can be produced at the center.

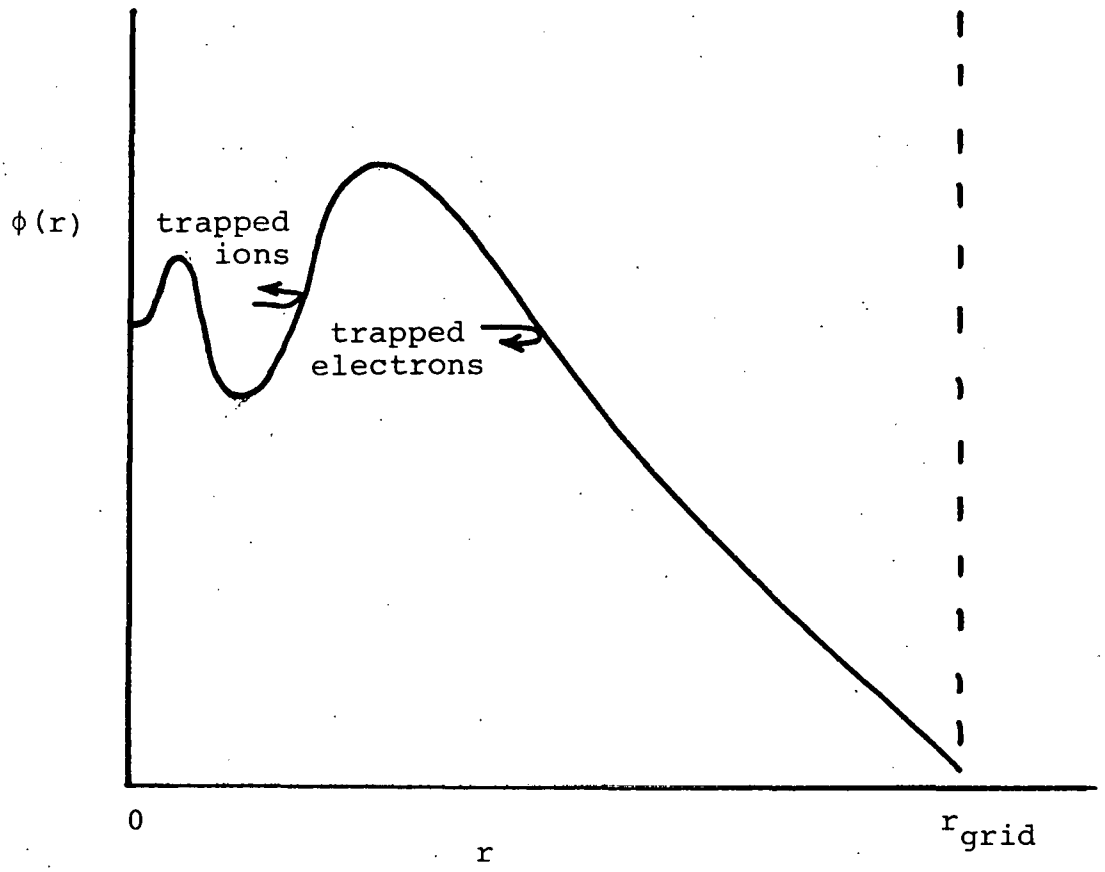

Fig. 2. The concept of multiple potential wells inside the grid of an electrostatic-inertial plasma confinement device.

indeed be formed.[5,6] However, overheating of the grid wires remains a serious problem.

One way to reduce the heat load from charged particle bombardment of the grid wires is to shield them magnetically by passing high currents through them, as illustrated in Fig. 3. If electrons are injected through the grid wires, very few will contact the grid wires directly. Some electrons will gradually become trapped in the magnetic field and diffuse to the grid wires, but this process is many orders of magnitude slower than direct bombardment. Such a scheme has been proposed for a fusion reactor.[7,3] The same scheme has also been developed from a different direction, namely, from open magnetic confinement systems.

Minimum-B magnetic confinement systems offer good MHD stability, but suffer from rapid plasma loss along magnetic field lines. Confinement times in adiabatic magnetic mirror devices are typically on the order of ion-ion scattering times, which makes $Q \leq 1$, where Q is the ratio of fusion power to injection power. Confinement times in non-adiabatic devices, such as cusps and open-ended SURMAC (to be discussed later) are $\tau \sim 4V/v_i S_L$, where v_i is the ion speed, V is the plasma volume, and S_L is the total loss hole area. This time is typically tens to hundreds of bounce times back and forth inside the central field-free (high-beta) region. For cusp confinement, the loss area through each circular cusp with radius R is $2\pi R(2\delta)$, where δ is the effective half-width of the cusp gap through plasma is lost. If $\delta \sim \rho_i$ (the ion Larmor radius), then unfeasibly large R and B would be required for a reactor. If $\delta \sim (\rho_e \rho_i)^{1/2}$ (a hybrid gyroradius) as indicated

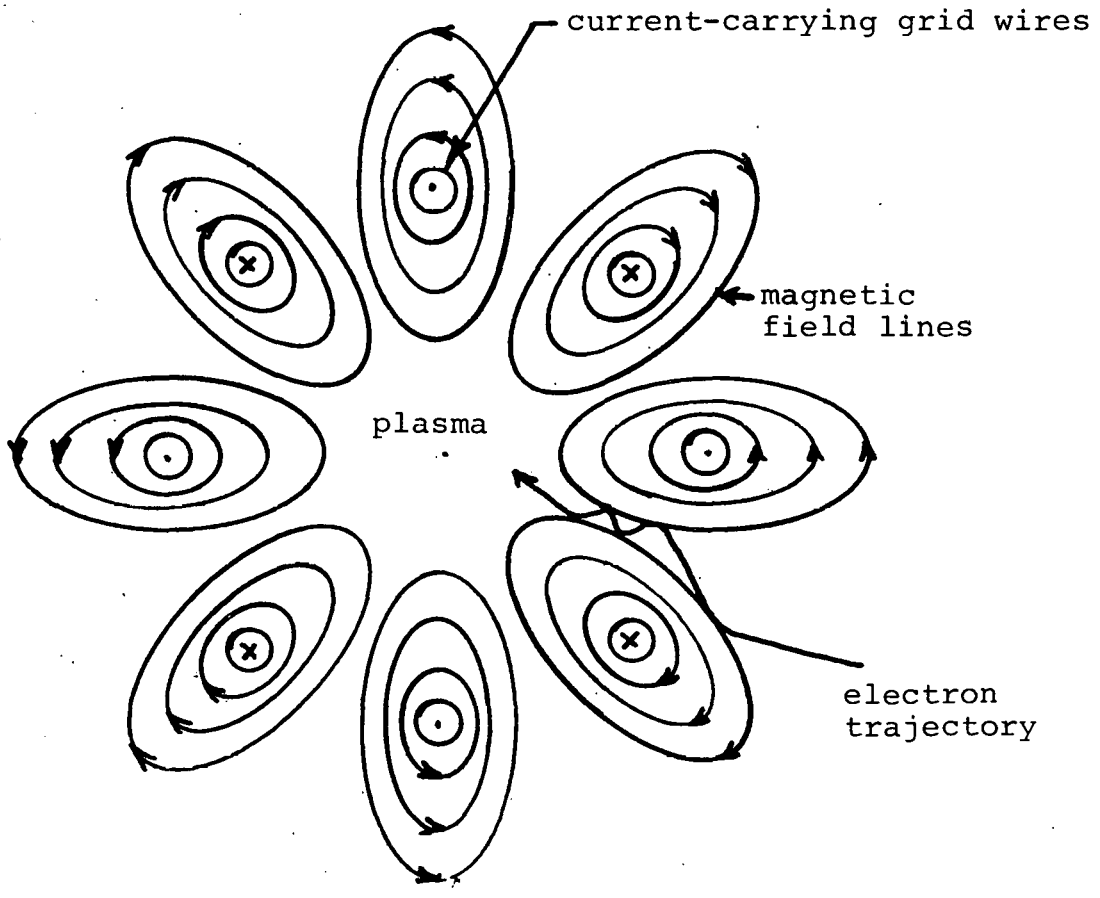

Fig. 3. Magnetic shielding of the grid of an electrostatic plasma confinement device.

in some recent experiments, then a reactor is feasible, but very high magnetic fields and large radii are needed.[8] For an open-ended SURMAC device, the minimum size end loss holes require a very large plasma volume to attain adequate τ. Thus it is desirable to find a means for plugging end losses from mirrors, cusps, and open-ended SURMAC devices in order to attain high Q ($Q \gtrsim 5$) without requiring extremely large R or B.

Several means of Q-enhancement for open magnetic confinement systems are being studied: radiofrequency (rf) plugging, field-reversed configurations, Tormac, multiple mirrors, the Tandem Mirror, and electrostatic plugging. Electrostatic plugging of cusps was proposed to reduce the loss rate of plasma flowing along magnetic field lines out the cusp gaps.[7] This is achieved by using electrodes in the cusp region to repel escaping electrons, and thus to control the plasma potential.[3,7,9-12]

If the plasma potential is highly negative, relative to the walls, the ions will be confined electrostatically, regardless of the configuration of the magnetic field or the size of their Larmor radius. Only electrons will be energetically able to pass through the narrow cusp gaps (plus a few ions in the high-energy tail of the Maxwellian), so the width of the untrapped electron stream flowing through the cusp gap will be $\delta \sim \rho_e$.

Early experiments with "electromagnetic traps" (electrostatically plugged cusps) showed that the electron confinement time increases by over three orders of magnitude when the plugging voltage is turned on, that the rate of electron loss across the magnetic field is similar to that expected from classical diffusion,

and that the plasma density increases proportional to B^2.[3] Further experiments have shown that the ion temperature scales linearly with applied voltage, and that a deep, negative potential well can be sustained for the duration of the experiment (many msec).[13]

Theoretical analyses indicate that the particle loss times along magnetic field lines are on the order of their self-collision times multiplied by $\exp(\phi_j/T_j)$, where ϕ_j is the electrostatic potential barrier confronting escaping particles, T_j is their temperature, and j = i or e.[14-17] For a given chamber size and magnetic field strength in the cusps, the probability of an electron's flying out through the cusp gap diminishes with increasing order of the multipole, that is, with increasing number of cusps.[18]

Those electrons which do succeed in entering the cusp gaps are accelerated by the positive applied voltage there, so their density drops.[19] Because of this effect, the electron density in the plasma can be significantly greater (by a factor of about 3) than the electron density in the cusp gaps.

The shear of the electrons' $\vec{E} \times \vec{B}/B^2$ drift velocities in the line cusp region gives rise to the diocrotron instability. Recent theoretical and experimental studies indicate that this instability is the main limitation on electron density and transport rates in the cusp gap.[20] The long-wavelength mode, which begins at low densities, can be stabilized by a conducting wall placed very close to the electron stream in the cusp gap. This conducting wall can be the positive plugging electrode (anode). The short-wavelength mode is insignificant at low densities, but limits the plasma density in the line cusp such that $q \equiv \omega_p^2/\omega_{ce}^2 \leq 0.2$ there.

Thus, electrostatic plugging has evolved from two directions: magnetic shielding of grids in spherical electrostatic confinement systems, and electrostatic plugging of end losses from open-ended magnetic confinement systems.

HOW ELECTROSTATIC PLUGGING IS SUPPOSED TO WORK

A toroidal cusp is illustrated in Fig. 4. High voltage electrode rings are placed in each of the cusp gaps, as shown. The anodes are biased positive, and the cathodes negative. Operation of the confinement system depends primarily upon the voltage ϕ_A applied between the cathode and anode, and not upon the relative location of the external "ground" potential. Either the cathodes, or the anodes, or neither, may be grounded.

In vacuum, the interior of the device will be near the anode potential (dashed curve). Plasma may be produced by electron beam injection into low-pressure gas, by rf heating, by plasma gun injection, by laser-pellet heating, by neutral beam injection, etc. Electrons going out through the cusps are reflected by the negative voltage of the cathode, but the exiting ions are not confined. They either strike the anodes, or else are accelerated into the cathodes. This initial poor ion confinement and good electron confinement results in loss of some ions, but almost no electrons, so that a charge imbalance is set up. The plasma develops a slight negative charge, due to the excess of electrons, and the plasma potential becomes negative relative to the anodes (the smooth curve of Fig. 4). If the anode gaps are narrow enough that their potential is not entirely shielded out by the plasma in the anode regions, then the potential there will be near the anode

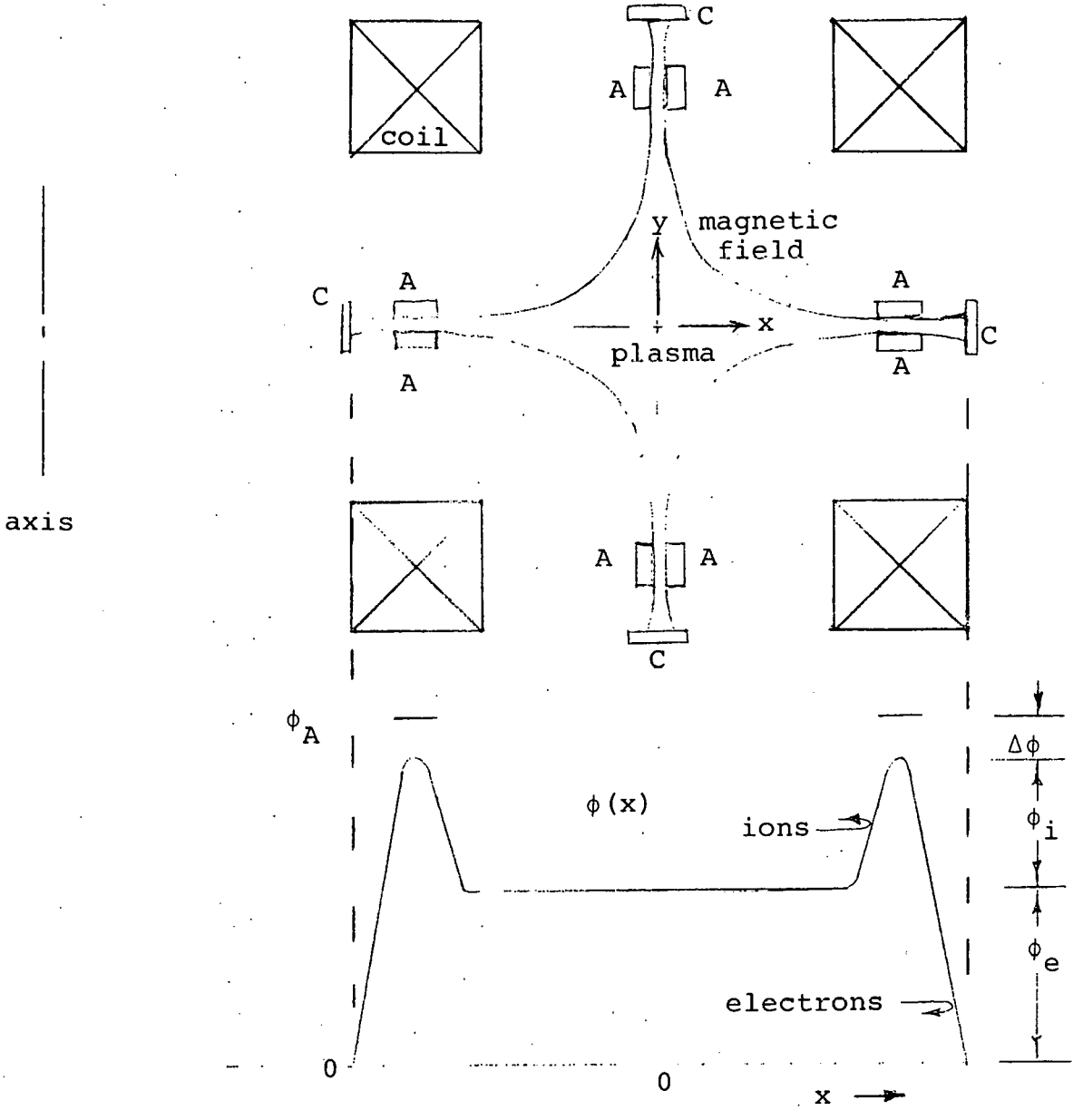

Figure 4. Electrostatic plugging system, and resultant potential distribution.

potential, and higher than the plasma potential, forming a potential hill ϕ_i for the remaining ions. Only a slight fractional charge imbalance is required to set up a potential hill many kV high. Now only ions with kinetic energies greater than $e\phi_i$ can escape along the magnetic field lines out the cusps. The two-dimensional potential distribution is illustrated in Fig. 5. The potential is saddle-shaped in the anode regions, with the saddle point lying an amount $\Delta\phi$ below the anode potential. The potential hill for ions trying to get to the walls (at anode potential) is even higher, so most ions will go out through the cusps (this is similar to "selective leakage" from mirrors) as soon as they acquire enough energy to overcome the barrier ϕ_i; very few ions will be confined long enough to get the energy required to overcome the barrier $(\phi_i + \Delta\phi)$ and get to the walls. Thus, the ions are electrostatically confined in a negative electrostatic potential well produced by a slight charge imbalance. It does not matter how large the ion Larmor radius is, because the ions will be electrostatically reflected in the boundary layer. Free streaming of electrons from the anode regions along the plasma boundary field lines will tend to maintain density distributions similar to those of the anode regions, except for the modifications imposed by differences in electrostatic potential. The existence of a potential difference along the magnetic field lines is made possible by the boundary condition that the walls are very close to the center of the plasma in the anode gaps, but very far from the plasma center along most of the boundary.

The central plasma region is free of both electric and magnetic fields, is uniform in density and temperature, and is

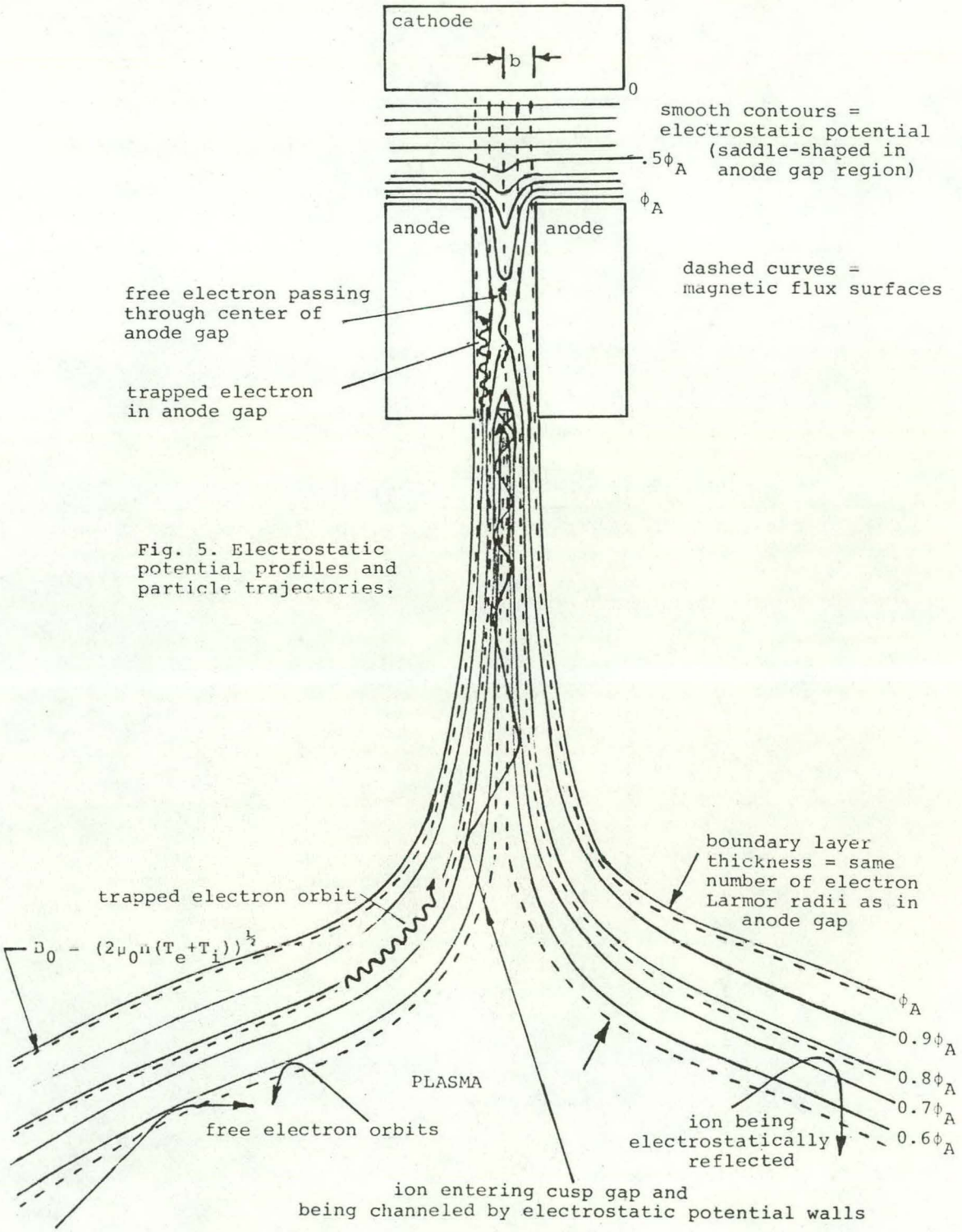

Fig. 5. Electrostatic potential profiles and particle trajectories.

surrounded by a thin boundary layer. The thickness of the boundary layer can be determined by flux-matching from the anode regions. The outer flux surface is the surface along which electrons are scraped off by the anodes. The inner boundary flux surface is that surface along which cold, untrapped plasma electrons are reflected.

Electrons can be trapped by the magnetic boundary layer. These electrons, which cannot enter the field-free region, are called "magnetically trapped". Another class of electrons consists of those electrons which have energies such that they are unable to enter the field-free central plasma region, as illustrated in Fig. 6. These electrons are called "electrostatically trapped". One source of electrostatically-trapped electrons is from ionization of incident neutral gas atoms along the slope of the potential well.

The anode gap half-width is typically $b \sim 3\text{-}10\ \rho_e$, so the entire plasma boundary should have a thickness of 3-10 Larmor radii, with the Larmor radius increasing away from the anodes, due to the decreasing magnetic flux density. The electron Larmor radius along the plasma boundary $\rho_o = \rho_e(B/B_0)$, where ρ_e is the Larmor radius in the cusp gap, B is the magnetic induction in the cusp gap, and B_0 is the induction along the plasma boundary. For a reactor, $b \sim 1$ mm, and the boundary layer thickness is on the order of 5 mm.

There are two sources of electrons: free (untrapped) electrons from the cathodes, and trapped electrons from ionization of incident neutral gas. (Very few of the electrons produced by ionization will be produced in a location where they are not trapped.)

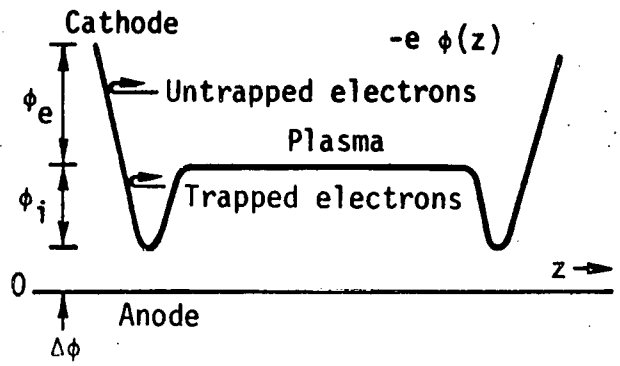

Fig. 6. Electron potential energy diagram.
(from Ref. 21)
This diagram represents the potential energy along magnetic field lines.

The free electrons will circulate back and forth through the plasma, occasionally passing out through the anodes and being reflected back in by the potential hill ϕ_e. There is, of course, mixing between the two electron groups: Coulomb collisions and E-field fluctuations can cause diffusion in velocity space, so that trapped electrons can become heated and detrapped, and free electrons can be cooled and trapped.[21,22]

There are two main free-electron loss processes: diffusion in velocity space over the potential barrier ϕ_e, and trapping by the magnetic field with subsequent diffusion to the anodes. By making the applied voltage ϕ_A sufficiently large, the loss rate along the magnetic field lines can be made arbitrarily small. It appears that $\phi_A \sim 300$ kV will be adequate.[21] Magnetic trapping of free electrons and diffusion are series processes. The total hot-electron cross-field confinement time is the sum of the trapping time plus the diffusion time.

Electron energy is supplied from the plasma source: electron beam injection, neutral beam injection, rf heating, etc. It is dissipated by thermal conduction, convection, radiation, and friction with the ions. The convection losses are essentially the same as the particle loss rates weighted by the average energy carried out by electrons escaping along and across the magnetic field.

Ions are produced by ionization of incident neutrals, usually along the slope of the potential hill, since the neutral atom mean free path is typically comparable to the thickness of the boundary layer. The resultant ions are accelerated as they

fall down the hill into the plasma region. This heating process partially compensates for charge exchange losses. The bulk of ion heating comes from interactions with hot electrons. Ion energy is lost by charge exchange and by convection, as heated ions escape over the potential hill ϕ_i.

THEORY

Magnetic Trapping Time

Typical particle trajectories of ions and electrons are illustrated in Fig. 5. The electrons travel in straight lines in the field-free region of the plasma. They are magnetically reflected off the boundary layer. In order to become magnetically trapped and diffuse across the magnetic field, they must undergo a Coulomb collision or scattering interaction with electric field fluctuation, which carries them across the velocity-space trapping boundary during the brief time that they are passing in and out of the boundary layer.

The average time it takes the free electrons to become magnetically trapped has not been accurately calculated yet. A procedure for calculating it and a rough estimate of the integral involved will be discussed here.

Consider a planar plasma-magnetic field boundary layer with the z axis chosen parallel to B and the x axis perpendicular to the boundary, as shown in Fig. 7. The effect of collisions in the boundary layer is illustrated in Fig. 8, which shows one trajectory in which an electron has become trapped as a result of a collision. The problem is to consider all the points along all possible trajectories of incident electrons, and determine what

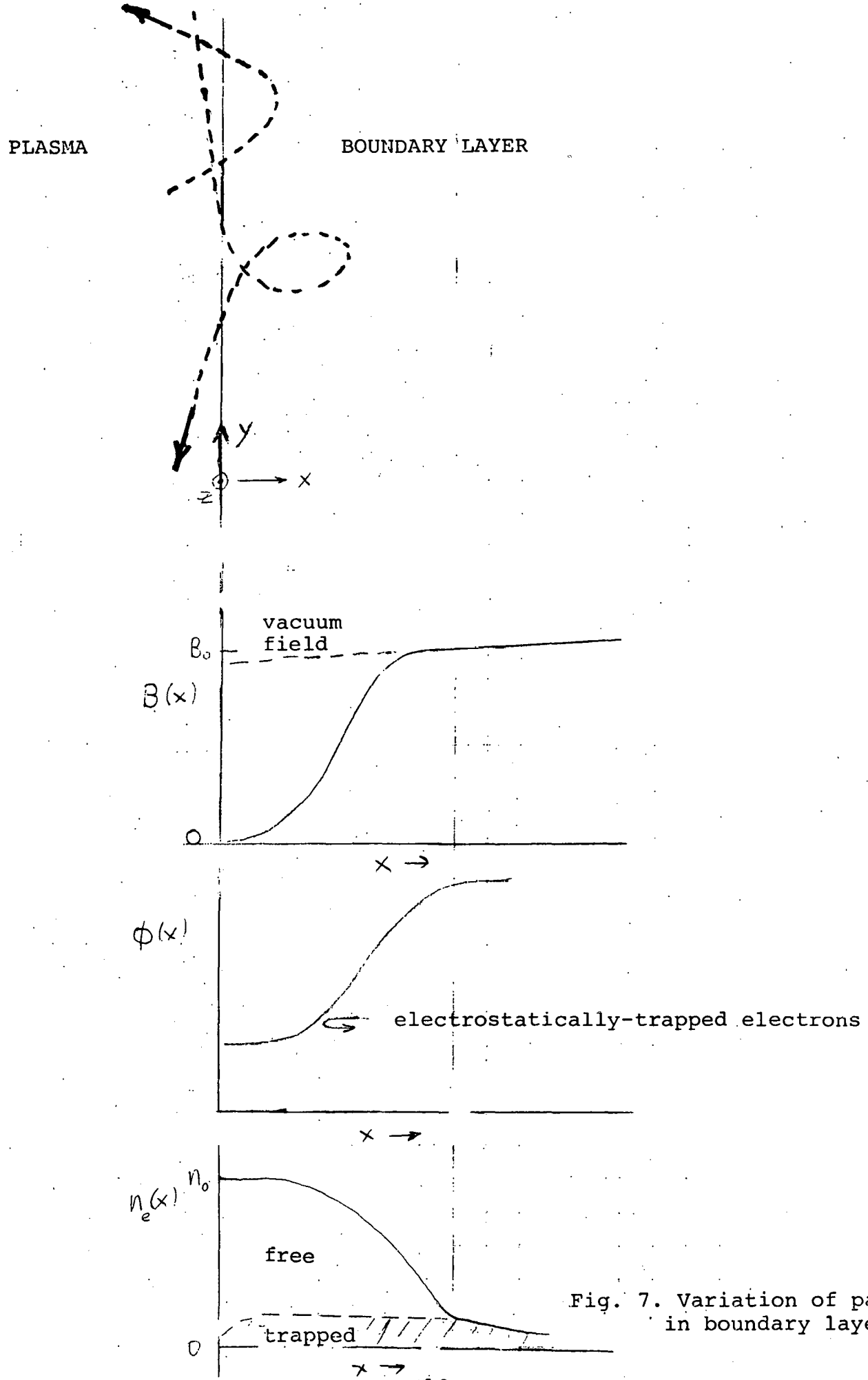

Fig. 7. Variation of parameters in boundary layer.

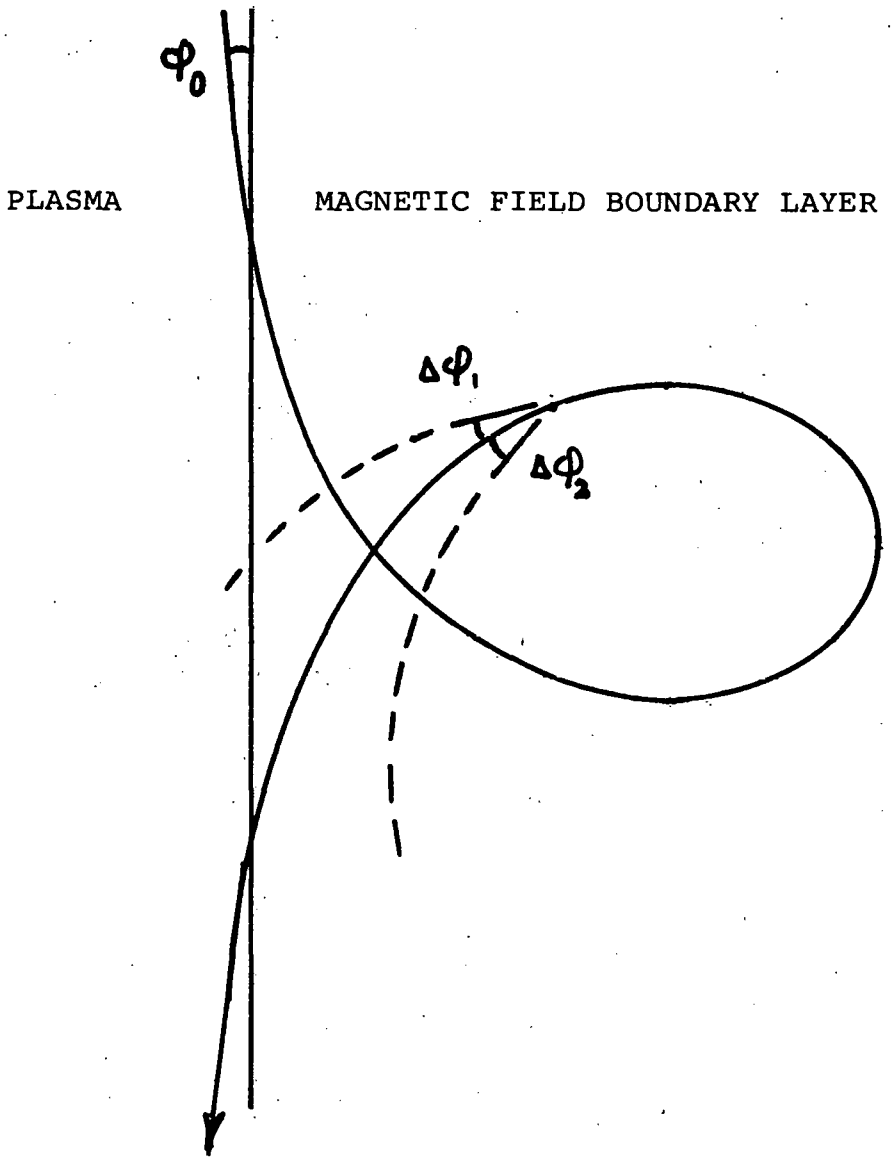

Fig.8 . Effects of Coulomb collisions in boundary layer. The deflection $\Delta\phi_2$ causes trapping, while $\Delta\phi_1$ does not.

fraction of these become trapped. The probability that a collision can cause trapping varies from point to point along each particle's trajectory, because the angles defining the trapping boundary change, and so does the collision frequency.

In addition to magnetic trapping, the electron may become electrostatically trapped by energy-loss collisions in the boundary layer, as can be seen from the electrostatic potential curve in Fig. 7.

The inverse trapping time may be written in the form

$$\tau_t^{-1} = \frac{\left[\begin{array}{c}\text{total number of electrons} \\ \text{incident per second}\end{array}\right] \left[\begin{array}{c}\text{probability of becoming} \\ \text{trapped along trajectory}\end{array}\right]}{(\text{total number of electrons in plasma})}$$

$$= \frac{S \int_0^{\pi/2} d\phi_0 \int_{-\infty}^{\infty} dv_{\parallel 0} \int_0^{\infty} dv_{\perp 0}\, v_{\perp 0} f(v_{\parallel 0}, v_{\perp 0}, \phi_0) \int_{\text{trajectory}} \frac{dl}{v_\perp(x)} \nu_c(x) \left[P_{et}(x, \phi_0, v_{\perp 0}, v_{\parallel 0}) + P_{emt}(x, \phi_0, v_{\perp 0}, v_{\parallel 0})\right]}{V \int_0^{\pi} d\phi_0 \int_{-\infty}^{\infty} dv_{\parallel 0} \int_0^{\infty} dv_{\perp 0}\, f(v_{\parallel 0}, v_{\perp 0}, \phi_0)} \quad (1)$$

where S is the plasma surface area, V is the plasma volume, ϕ_0 is the angle of electron incidence (Fig. 8), $v_{\perp 0}$ is the incident velocity component perpendicular to the magnetic field, $v_{\perp 0}$ is the incident vlocity component parallel to the magnetic field, $v_\perp(x)$ is the perpendicular velocity at position x, $\nu_c(x)$ is the Coulomb collision frequency, f is the electron distribution function in the plasma, $P_{et}(x,\phi_0,v_{\perp 0},v_{\perp 0})$ is the probability of a Coulomb collision's causing electrostatic trapping at x, and $P_{mt}(x,\phi_0,v_{\perp 0}, v_{\perp 0})$ is the probability of a Coulomb collision causing magnetic trapping at x. Computation of these probabilities is a complex geometrical problem, since they depend on the electron's velocity components, position in the boundary layer, and condition of the

field particles. Because of the multiple small-angle scattering nature of Coulomb collisions, the concept of an electron's trajectory being perturbed by just one collision is itself invalid. The probabilities P_{et} and P_{mt} are large only for electrons with very small ϕ_0 (near grazing incidence). The Monte Carlo method[23] may be useful in evaluating Eq. (1).

An approximate value of τ_t, due to Moir[24], is found by considering $\Delta\Theta$ rms, the rms value of deflection experienced by electrons during their brief transit in and out of the boundary layer, which lasts a time $t_1 = 2\pi m_e/eB_0$, where

$$B_0 = \left[2\mu_o n_e (T_e + T_i)\right]^{1/2} \tag{2a}$$

Assuming that the incident electrons are isotropically distributed and undergo deflections of $\Delta\Theta_{rms}$, about half of those incident at angles smaller than $\Delta\Theta_{rms}$ will be deflected in the right directions to become trapped. The fraction of electrons incident at angles in the x-y plane smaller than $\Delta\Theta_{rms}$ is roughly $(\Delta\Theta_{rms}/2\pi)$, so the fraction of incident electrons trapped is approximately $\Delta\Theta_{rms}/4\pi$. The trapping time may be found from the particle balance equation

$$n_e V/\tau_t = (1/4) n_e v_e S(\Delta\Theta_{rms}/4\pi) + (1/4) n_e v_e S(t_1/\tau_{90}) \tag{2b}$$

where v_e is an average electron speed and τ_{90} represents the 90° electron-ion scattering time. The second term on the right, which represents trapping by a single large-angle deflection, is much smaller than the first, and may be ignored. The value of $\Delta\Theta_{rms}$ attained during the transit time t_1, may be estimated from Eqs. (8.18) and (8.19) of Ref. (25), which gives

$$\Delta\theta_{rms} = \left(\frac{t_1}{\tau_\theta}\right)^{\frac{1}{2}} = \left[\frac{n_e e^3 \ell n \Lambda}{2 B_o \varepsilon_o^2 m_e V_e^3}\right]^{\frac{1}{2}} \quad (3)$$

where ε_0 is the permittivity of free space, τ_θ is an angular relaxation time, and $\ell n\Lambda$ is the Coulomb logarithm. Combining Eqs. (2) and (3), and using $V/S = r_p/2$, where r_p is the radius of the cylindrical plasma, we get

$$\tau_t = \frac{8\pi r_p}{V_e \Delta\theta_{rms}} = 8\sqrt{2}\,\pi\,\varepsilon_o\, r_p\, (M_e V_e B_o/n_e e^3 \ell n\Lambda)^{\frac{1}{2}} \quad (4)$$

This equation gives trapping times which are short compared to diffusion times across the magnetic field (to be discussed in the next section). If this estimate is correct, it means that the trapping time is negligibly short.

Confinement Time

The electron energy confinement time may be expressed in terms of energy loss rates along the magnetic field and across the magnetic field:

$$\tau_{Ee} = (\tau_{E\parallel}^{-1} + \tau_{E\perp}^{-1})^{-1} \quad (5)$$

The energy loss time along the magnetic field has been calculated by Sizonenko and Stepanov[16] to be

$$\tau_{E\parallel} = (\tau_{ee}\phi_e/\tau T_e)^{\frac{1}{2}} \exp(\phi_e/T_e)\tau_{ee} \quad (6)$$

where ϕ_e is the electrostatic barrier confronting escaping electrons (Fig. 3), T_e is the electron temperature, τ_{ee} is the electron-electron scattering time, and

$$\tau \equiv (r_p S/S_g v_m \xi) \quad (7)$$

is the average time it takes an electron in the plasma with speed $v \geqq v_m$ to pass through the "geometric" mirrors and impinge on the cathode. Here S_g is the plasma surface area, S_g is the surface area subtended by the anode gaps, $v_m \equiv \left(2e\phi_e/m_e\right)^{1/2}$, and ξ is the fraction of electrons with $v \geqq v_m$ which can get through the anodes without being mirror reflected and reach the cathodes. Various estimates of τ are given in Ref. (16) for different limiting cases of magnetic field variations and collisionality. Here we will assume $\xi \sim 0.8$.

For a cylindrical multipole plasma with N cusps, the area subtended by the magnetic cusp gaps is approximately

$$S_g/S \simeq \frac{N2\rho_L}{2\pi r_p}$$

where ρ_L is an average Larmor radius of fast electrons entering the cusp gap. We will assume that two-thirds of the energy is perpendicular to the magnetic field, so that

$$\rho_L = (2/3)^{1/2} v_m m_e/eB_0$$

where $B_0 = \left(2\mu_0 n_e(T_e + T_i)\right)^{1/2}$ is the magnetic field at the plasma boundary. With these approximations, τ may be written

$$\tau \sim \pi 3^{1/2}\, B_0 r_p^2/2\xi 2^{1/2} N\phi_e \sim 2.4\, B_0 r_p^2/N\phi_e. \qquad (3)$$

An alternative equation for $\tau_{E\ell}$ may be found from the results of Pastukhov (17). Since the energy $e\phi_e$ is recovered directly as electricity at the cathodes, the parallel energy

confinement time is defined in terms of the functions calculated by Pastukhov to be

$$\tau_{E\parallel} = \frac{-1.5\ n_e T_e}{1.5\ \frac{d(n_e T_e)}{dt} - e\phi_e \frac{dn_e}{dt}} \tag{9}$$

Using Eqs. (21)-(23) of Ref. (17), this becomes

$$\tau_{E\parallel} = 1.5\ \tau_{ee}\ g(R)\ \exp\left(\phi_e/T_e\right)\left(\phi_e/T_e\right)\left(1 - T_e/\phi_e + \ldots\right) \tag{10}$$

where τ_{ee} is the electron-electron scattering time and $g(R)$ is a function of the mirror ratio R. For the present nonadiabatic case we take $R = 1$, and $g(R) = 2.4$. Eqs. (6) and (10) give estimates of $\tau_{E\parallel}$ which have slightly different variations with $\left(\phi_e/T_e\right)$.

The cross-field energy loss time may be written

$$\tau_{E\perp} = \left[\left(\tau_{cond}\right)^{-1} + \left(\tau_t + \tau_d\right)^{-1}\right]^{-1} \tag{11}$$

where τ_{cond} is the time for heat loss by conduction and τ_d is the characteristic time for electron loss by diffusion. Radiation losses are not included in the energy loss time defined by Eq. (11). For a high-beta, large-volume cusp plasma (such as in a multipole cusp) the diffusion time is [21]

$$\tau_d = Cr_p b/\rho_e^2 \nu \tag{12}$$

where ρ_e is the average electron Larmor radius in the line cusp region; b is the half-width of the anode gap; ν is the effective momentum-transfer collision frequency of the electrons, including collisions with ions, neutrals, and E-field fluctuations; and $C \sim 0.1$ is a numerical coefficient depending on the shape of the magnetic flux surfaces.

For low-beta, magnetized cusp plasmas (such as spindle cusps with low plasma pressures) the diffusion time may be estimated from the equation[26,27]

$$\tau_d = (b - \rho_e)^2/\rho_e^2\nu. \tag{13}$$

Here b must be interpreted as the distance from the midplane of the line cusp to the scrape-off flux surface, which may be inside the line cusp anodes in some cases (such as when the electrons travelling along an inner flux surface can get scraped off by the point cusp anode).

The energy loss time from heat conduction is roughly[21]

$$\tau_{cond} \simeq 1.5\ \tau_d. \tag{14}$$

In order to wall-stabilize the long-wavelength diocotron instability, b must not be much larger than the size of the electron stream in the anode regions (a few ρ_e).[20] Present experiments have $b/\rho_e \sim 3\text{-}10$. We will assume that stability can be maintained, provided that

$$b/\rho_e \lesssim 5. \tag{15}$$

Inserting Eq. (15) into Eq. (12), we find that

$$\tau_d \simeq .5\, r_p/\rho_e \nu. \tag{16}$$

Numerical estimates of Eqs. (4), (16) indicate that $\tau_t \ll \tau_d$. In the limit of high applied voltage ϕ_A, $\left(\tau_{E\perp}/\tau_{E\parallel}\right) \ll 1$, as will be discussed below. For this case, we find from a combination of Eqs. (5), (11), (12), (14), and (16) that

$$\tau_E \simeq \tau_{E\perp} \simeq \frac{0.3\, r_p}{\rho_e \nu}. \tag{17}$$

For numerical evaluation of this equation, we will consider the case in which $T_i \sim T_e$ and electron-ion collisions are dominant. Then

$$\nu \sim \nu_{ei} = 3.7 \times 10^{-15} n/T_{ek}^{3/2} \tag{18}$$

where T_{ek} is the electron temperature in keV and the density n is in m^{-3}. In these same units, the electron Larmor radius is

$$\rho_e = \left(2m_e 1000 e T_{ek}\right)^{1/2}/eB \tag{19}$$

where B is in Tesla, and e is the electronic charge (C). After inserting Eqs. (18) and (19) into Eq. (17), we get

$$n\tau_E \sim 8 \times 10^{17} r_p B T_{ek} \left(m^{-3} sec.\right) \tag{20}$$

Eq. (20) gives the qualitative scaling to be expected in the limit where losses along the magnetic field lines are negligible. Now we will estimate how high the voltage must be to make those losses negligible, using Eq. (10) for $\tau_{E_\parallel}$.

$$\frac{n\tau_{E_\perp}}{n\tau_{E_\parallel}} \simeq \frac{8 \times 10^{17} \; r_p \; B \; T_{ek}}{3.6 \; C_{ee} T_{ek}^{3/2} y e^y \left[1 - \frac{1}{y}\right]} < 0.1 \tag{21}$$

where $C_{ee} = 5.3 \times 10^{14} m^{-3} keV^{-3/2} sec$ and $y = \phi_e / T_e$. After rearrangement, this becomes

$$e^Y (y - 1) > 4.2 \times 10^3 \; r_p B / T_{ek}^{1/2} \tag{22}$$

For example, consider the case $r_p = 2m$, $B = 5T$, $T_{ek} = 20$ keV. For this case, $e^Y (y - 1) > 9400$, or $y = 7.4$. Assuming $\phi_e \sim \phi_A / 2$, the required value of ϕ_A is about 300 kV. Because of the exponential function, large increases of $r_p B / T_{ek}^{1/2}$ can be compensated for by slight increases in Y.

Diocotron Oscillations

By definition, let $q \equiv \omega_{pe}^2 / \omega_{ce}^2 = \rho_e^2 / 2\lambda_D^2$, where ω_{pe} is the electron plasma frequency in the line cusp anode, ω_{ce} is the electron cyclotron frequency there, and λ_D is the Debye length. The ion density in the anodes is very small, because few ions are energetically able to reach the anode gap, and those which

can get through are lost at the cathodes after one pass (unless additional plugging electrodes are added). The negative electron space charge in the anodes depresses the electrostatic potential there by an amount $\Delta\phi$, and the resultant electric field produces an $\frac{\vec{E}\times\vec{B}}{B^2}$ drift in the $\pm y$ direction, as illustrated in Fig. 9. The shear of the drift velocity tends to produce the slip-stream or diocotron instability, which can cause rapid electron transport across the magnetic field to the anodes.

The long-wavelength diocotron instability can occur at very low values of q, on the order of 10^{-4}, which would limit the density to very low values. However, the long-wavelength modes can be stabilized by the presence of a conducting wall near the plasma.[20] It has been found experimentally that having one of the anodes within a few ρ_e of the electron stream is adequate to maintain stability.

The short-wavelength diocotron instability has a rate given by[28]

$$\gamma/\omega_{ce} \sim (q/2) \exp(-2/q) \qquad (23)$$

which is shown in Fig. 10. This instability is apparently insignificant for $q < 0.1$, and it is significant for $q > 0.2$.

The diocotron instability has been observed experimentally, and it appears to be the major limitation on plasma density. Instabilities due to two-stream interactions and drift waves have not been observed so far.

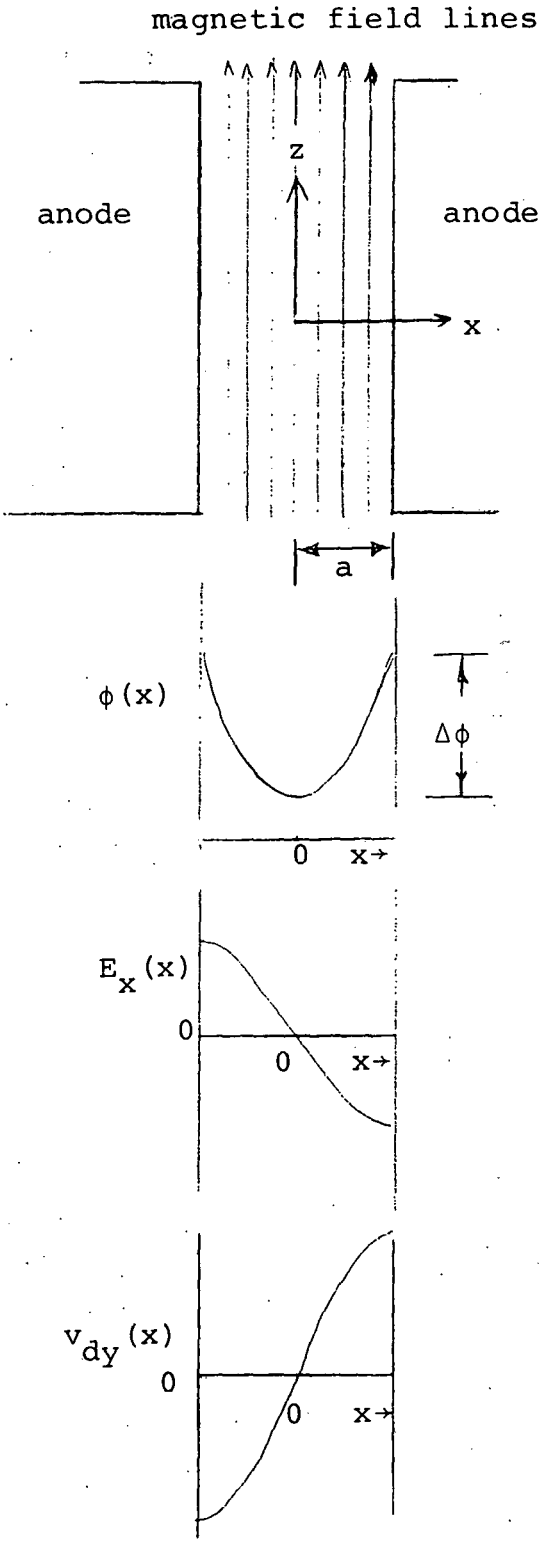

Fig. 9. Distributions of electrostatic potential, electric field, and electron drift velocity in the anode gap region.

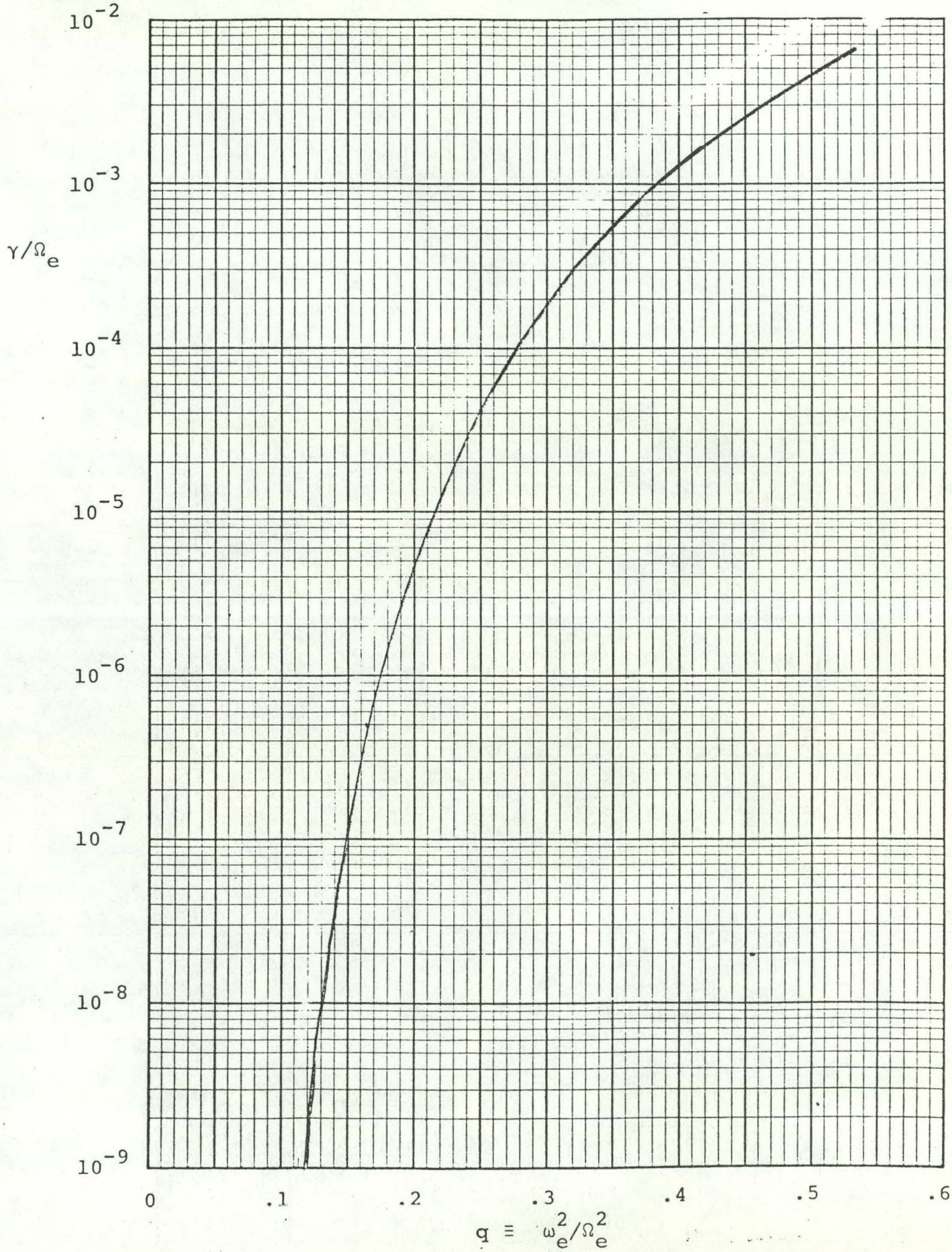

Fig. 10. Growth rate of the short-wavelength diocotron instability.

Electron Density

Assuming that the short-wavelength diocotron instability limit is $q \lesssim 0.2$ (for which $\lambda_D \lesssim 1.6\rho_e$), the resultant limitation on electron density in the line cusp anode is[13,20]

$$n_A \lesssim 0.2\, \varepsilon_0 B^2/m_e = 2 \times 10^{18}\, B^2 \quad \text{(SI units)}. \tag{24}$$

The electron density in the central plasma can be significantly higher, because plasma electrons are accelerated as they pass through the anodes. On the other hand, cold trapped electrons accumulating in the anode would raise the density there. Considering only electrostatic acceleration, the density ratio is[19]

$$n_e/n_A = \exp\left(\phi_i/T_e\right)\mathrm{erfc}\left(\phi_i/T_e\right)^{1/2} \tag{25}$$

where ϕ_i is the potential barrier for ions (Fig. 3). For typical parameters, the density ratio given by Eq. (25) is about 3. An approximate theoretical estimate of the density of cold trapped electrons indicates that their density is probably less than half the density of free plasma electrons streaming through the anodes.[21]

Plasma Potential

The plasma potential will adjust itself so that the electron and ion particle loss rates are equal. The ion and electron loss rates over their potential barriers can be estimated from the equations of Stix,[15] Sizonenko and Stepanov,[16] or Pastukhov.[17] Using the latter equations

$$dn_i/dt = S_i - n_i/\tau_i$$

$$= S_i - \left(n_i/\tau_{ii} g(R)\right) \exp\left(-Y_i\right)\left(1/Y_i\right)\left(1 + 1/2Y_i - 1/4Y_i^2 + \ldots\right) \quad (26)$$

where $Y_i = \phi_i/T_i$, $g(R)$ is again equal to 2.4, τ_{ii} is the ion self-scattering time, and S_i is the ion source from ionization. Recombination is negligible.

The ionization source term for electrons is also S_i. Electrons exiting over the potential barrier ϕ_e are subtracted from the electron beam injection current from the cathodes. The net current I can be either positive or negative, depending on whether the heating must be supplied by the electron beams or whether additional heating is available, as from rf. The electron particle balance equation is

$$dn_e/dt = S_i + I/eV - n_e/\tau_\perp . \quad (27)$$

By equating $dn_i/dt = dn_e/dt$, we can find the value of ϕ_i. (If fusion reactions are significant, another loss term must be added to Eq. 26). Knowing (or assuming) the spatial distribution of electrons in the anodes, we can solve the Poisson equation there for $\Delta\phi$, and also find $\phi_e = \phi_A - \phi_i - \Delta\phi$. Typically, ϕ_e is about half the applied voltage.

Temperatures

An energy balance equation for the electrons may be written[21]

$$1.5D(nT_e)/dt = I\phi_e/eV - 1.5nT_e/\tau_{Ee} - P_{rad} - 1.5n(T_e - T_i)/\tau_{eq} \quad (28)$$

where the "energy confinement time" τ_{Ee} defined previously includes only conduction and convection, P_{rad} is the radiative power loss, and the last term represents energy transfer to the ions. An energy balance equation for the ions may be written[21]

$$1.5d(nT_i)/dt = 1.5n(T_e - T_i)/\tau_{eq} + f_i S_m W_a - (1 - f_i) S_m 1.5T_i - n_i\phi_i/\tau_i \quad (29)$$

where f_i is the fraction of incident neutrals which are ionized (instead of causing charge exchange), S_m is the volume-averaged neutral input rate, W_a is the average energy acquired by ions formed along the slope of the potential well, τ_i is the ion confinement time defined in Eq. (26), and the effects of fusion reactions have been ignored. These equations are nonlinear, because the coefficients depend on the temperatures. They have been solved numerically for some cases. The resulting ion temperatures are typically about 5-15% of the applied voltage for the case of a plasma sustained by neutral beam injection[29] and about 5% of the applied voltage for a plasma sustained by electron beam injection.[21] The predicted electron temperatures are generally slightly higher than the ion temperatures, although they can be lower for the case of neutral beam heating.

EXPERIMENTAL RESULTS

Some parameters of recent experiments are listed in Table 1. All of these experiments are spindle cusps, due to financial limitations, although spindle cusps are the worst cusp geometry for plugging. The magnetic fields listed are B_r in the line cusp (the point cusp field is usually much stronger). In these experiments, the plasma is created by electron beam injection along magnetic field lines, with subsequent ionization of neutral gas.

Experimental plasma densities increase proportional to B^2, in accordance with Eqs. 24 and 25, as illustrated in Fig. 11. In this figure the lower line is a plot of n_A from Eq. 23. Experimental data for two experiments indicate that n_e/n_A is significantly higher than expected from Eq. 25.[20,30] The reason for this beneficial effect is not understood.

In comparing the theoretical confinement times given by Eqs. (3)-(14) with experimental data, there are two main uncertainties in the data: we do not know the exact values of T_e or p (neutral gas pressure) at which the data were taken. Even where pressure was measured experimentally, there can be significant variation between the gage and the edge of the plasma. Nevertheless, we can use estimated values of p and T_e to calculate confinement times, for comparison with measured confinement times. This is done for four experiments in Table 2. Numerical estimates indicate that the parallel loss processes are negligible for the cases of these experiments, so only cross-field losses are included

Table 1. Parameters of various experiments.
(Refs. 21,26,30-33)

	Missouri	Quebec	Kharkov	suggested experiment	reactor
B (kG)	3	4	10	15	70
ϕ_A (kV)	1	2	7	10	300
p (Torr)	10^{-5}	10^{-5}	10^{-7}-10^{-6}	10^{-7}-10^{-6}	10^{-7}-10^{-6}
n_e (cm^{-3})	3×10^{10}	4×10^{11}	5×10^{12}	10^{13}	10^{14}
T_e (keV)	(.03)*	(.1)*	~2	~2	30
T_i (keV)	(.003)*	(.01)*	1	1	20
τ_E (msec)	0.1	0.5	5	10	>1000
τ_{ee} (msec)	0.09	0.04	0.3	0.2	0.9

* estimated (not measured)

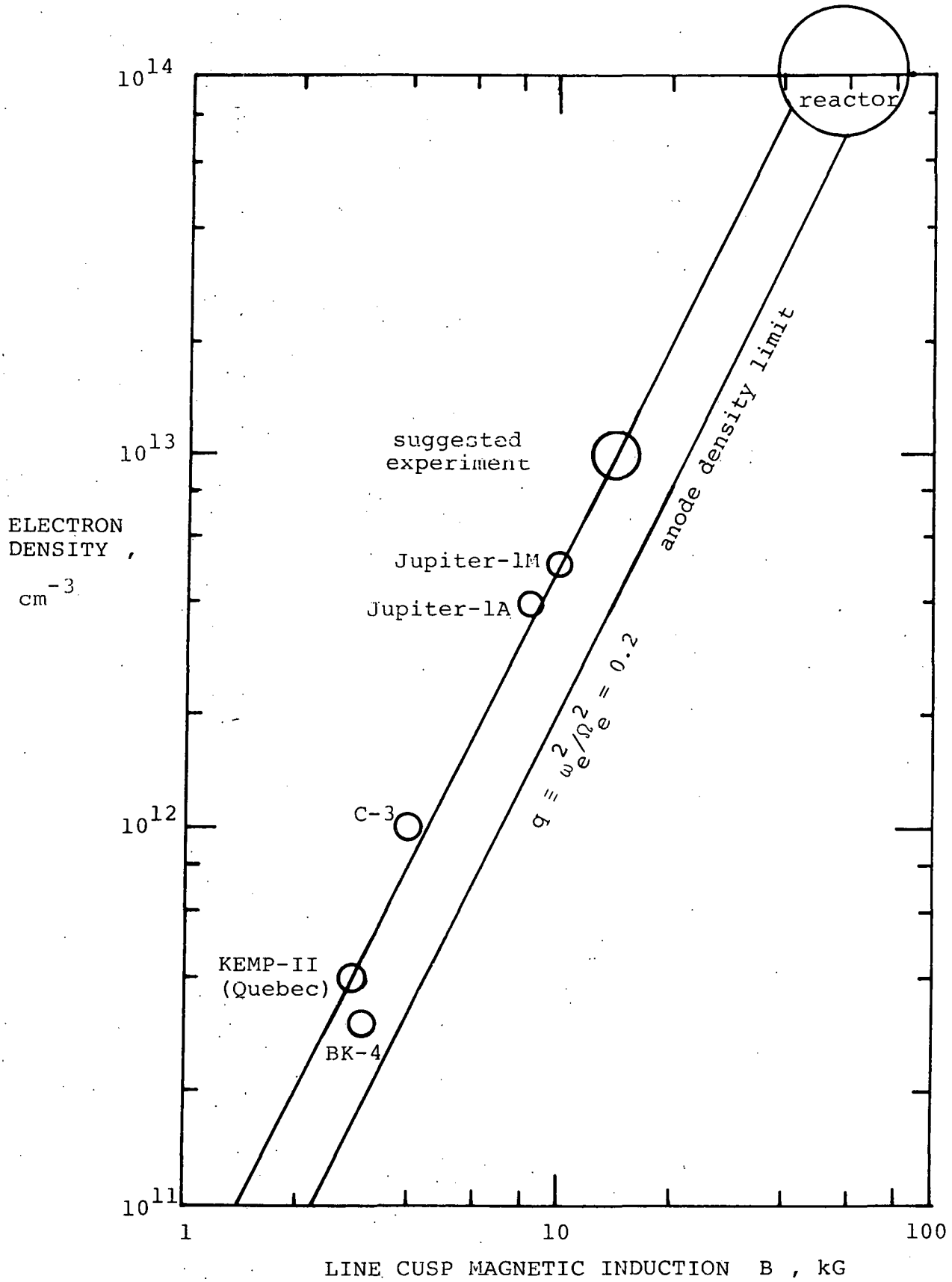

Fig. 11. Variation of plasma density with magnetic induction.

Table 2. Comparison of Theoretical $\tau_\perp$ and $\tau_{E\perp}$ with Experimental Confinement Times

		Misscuri[26]	Quebec[30,32]	Kharkov Jupiter 1-A[31]	Jupiter 1-M[31]
	ϕ_A(kV)	0.5	2	5	7
	B_z(T)	.5	1.0	4.5	3.0
	B_r(T)	.3	0.3	.85	1.0
ring anode radius	R(mm)	160	175	120	120
half-gap width	d_2(mm)	3	3.1	~ 1*	~ 1*
point anode radius	r_2(mm)	5	9.5	~ 9*	~ 9*
	$n(M^{-3})$	2×10^{16}	3×10^{17}	4×10^{18}	5×10^{18}
	T_e(keV)	~ .01*	~ .1*	~ 2*	~ 2*
	T_i(keV)	~ .001*	~ .01*	~ .8	~ 1
	p(Torr)	$\sim 10^{-5}$*	$\sim 3 \times 10^{-6}$*	$\sim 10^{-6}$*	$\sim 3 \times 10^{-7}$*

*Estimated; data not available

$b = \min\left[d_2 \quad \frac{r_2^2 B_z}{2RB_r}\right]$	0.13 mm	0.64	1.0	1.0
$\nu_{em} = 5 \times 10^9 p \ (Sec^{-1})$	5.9×10^4	1.8×10^4	5.9×10^3	1.8×10^3
$\nu_{ei} = \frac{1.37 \times 10^{-15} n}{T_e^{3/2}\,(keV)} \ \nu(Sec^{-1})$	2.74×10^4 8.64×10^4	1.3×10^4	1.9×10^4	2.4×10^3

Table 2. (continued)

	Missouri[26]	Quebec[30,32]	Kharkov Jupiter 1-A[31]	Jupiter 1-M[31]
ρ_e (mm)	0.036	0.084	0.18	0.15
$r_p \approx \frac{Rv2\mu_0 n(T_e+T_i)}{B_r}$ (mm)	0.15	2.0	9.0	9.3
τ_d (msec)	.080	1.4	2.7	7.6
$\tau_\perp$ (msec)	.048	0.77	2.0	14.8
$\tau_\perp$ (msec)	0.13	2.2	---	---
$\tau_{E\perp}$ (msec)	---	---	2.0	7.6
exp. meas. (msec)	.09 ± .03	.9 ± .1	1 ± .5	5 ± 2

in Table 1. Two of the experiments measured energy confinement times, while the other two measured density decay times. The density decay times are therefore compared with the cross-field particle confinement time $\tau_\perp = \tau_t + \tau_d$.

The plasma potential relative to grounded anodes was measured by the time of flight of a pulsed heavy ion beam injected through the plasma along magnetic field lines.[13] Data from this measurement are shown in Fig. 12. Initially a virtual cathode is formed ($\phi_e \sim 0$). Then, as plasma ions from ionization of neutral gas accumulate, the potential rises up to its equilibrium value, where it stays for the duration of electron beam injection (20 msec). After the end of injection, the plasma potential shifts to a new equilibrium value (because I goes to zero in Eq. 27), and then finally returns to ground potential when the plasma is lost. These data were taken at 10^{-6} Torr. At 10^{-5} Torr, the potential well washes out after about a millisecond probably because cold, trapped electrons trigger the diocotron instability (reducing $\tau_\perp$ in Eq. 27). Experimental values of plasma potential are fairly consistent with theoretical predictions.[34]

Experimental observations of diocotron oscillations in the line cusp indicate the following: (1) The frequency of the oscillations is proportional to applied voltage and inversely proportional to magnetic field strength, in accordance with theoretical expectations.[20,35] (2) The growth rate of the instability is proportional to neutral gas pressure, and thus to the density of cold electrons produced by ionization, as expected. (3) By

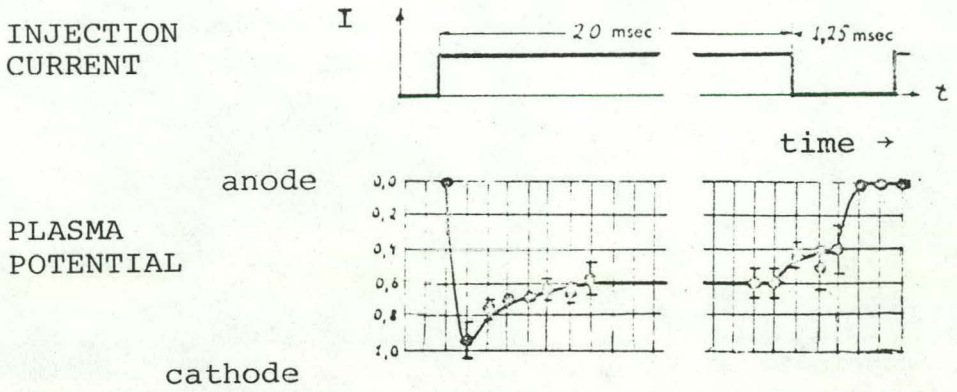

Fig. 12. Plasma potential as a function of time (Ref. 13).

segmenting the ring cusp cathode, the relative ion currents as a function of azimuthal angle have been measured. These measurements indicate that the long-wavelength instability has a mode number $m = 1$ or 2 (the number of wave periods of the wave around the circumference of the ring). Higher mode numbers (shorter wavelengths) are apparently more stable. The theoretical and experimental aspects of diocotron instabilities in electromagnetic traps are summarized in Ref. (20). No other microinstabilities have been observed during plasma observation periods of about $10\ \tau_{ee}$.

Both electron and ion energy spectra have been measured with gridded electrostatic energy analyzers mounted in point cusps. The electron energy distribution resembles a Gaussian distribution centered at an energy between the cathode and plasma potentials.[13]

The ion energy spectra were measured with a drift mass spectrometer combined with an electrostatic ion-energy analyzer. A plot of the ion energy distribution for $\phi_A = 2.5$ kV is shown in Fig. 13. The distribution appears to have two Maxwellian components. The higher-temperature component is believed to be caused by the initial formation of the potential well. The average energy of all the ions increases linearly with applied voltage, as shown in Fig. 14, with a slope $\bar{W}_i \simeq 0.18\ \phi_A$.

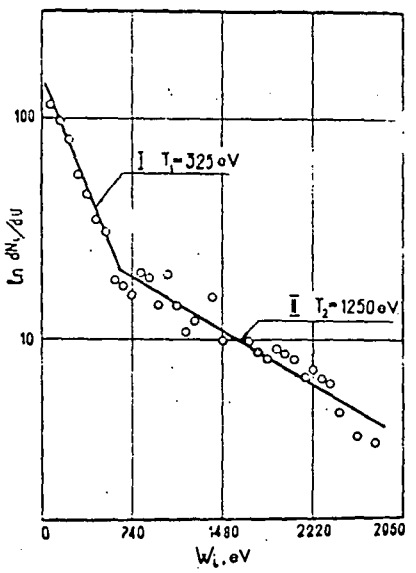

Fig. 13. Measured ion energy spectrum, for the case in which ϕ_A = 2.5 kV. (Ref. 13)

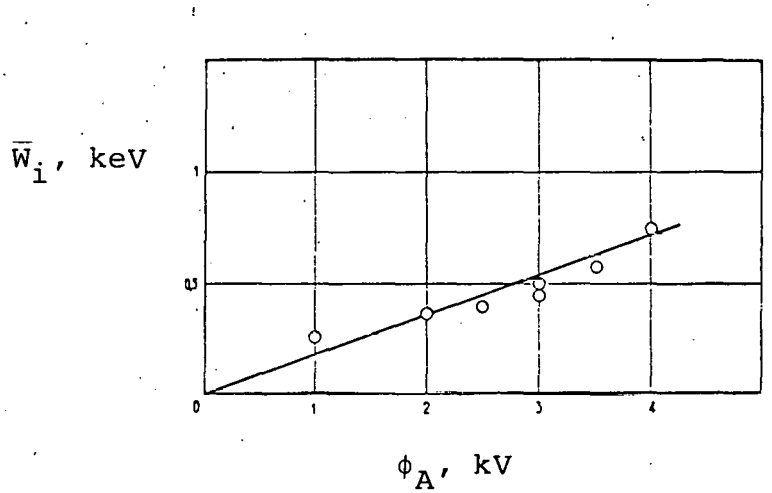

Fig. 14. Variation of mean ion energy with applied voltage (Ref. 13).

REACTOR CONCEPTS

Various cusp geometries suitable for electrostatic plugging are illustrated in Figs. 15 and 16. Mirror geometries, such as a Yin-Yang field, are also suitable for electrostatic plugging, but the plasma volume between the anode-bounded flux surfaces is much smaller than for cusp systems, and therefore probably less economical.

A Soviet fusion reactor concept, based on a spherical multipole cusp, is shown in Fig. 17. The sphere has the best surface-to-volume ratio, and the spherical electrode arrangement might provide some spherical focussing of charged particles. If effective, such focussing would increase the central plasma density and decrease the required magnetic field in the cusps. However, electron-electron scattering might tend to nullify the effects of focussing. A reactor design involves an electrostatically-plugged toroidal hexapole cusp, as illustrated in Fig. 18. The variations of the reactor Q = (fusion power)/(injection power) with applied voltage and magnetic field are shown in Figs. 20 (a,b) for the case in which the plasma is sustained solely by electrons from the cathodes. These were calculated using global particle and energy balance equations like Eqs. (26)-(29) with added terms for fusion reactions and impurity effects. These curves are speculative, in view of the uncertainties in the underlying theory.

Some representative parameters of this reactor design are listed in Table 3. Two power flow diagrams for this reactor are shown in Fig. 21, assuming that the startup takes 10 sec, fusion

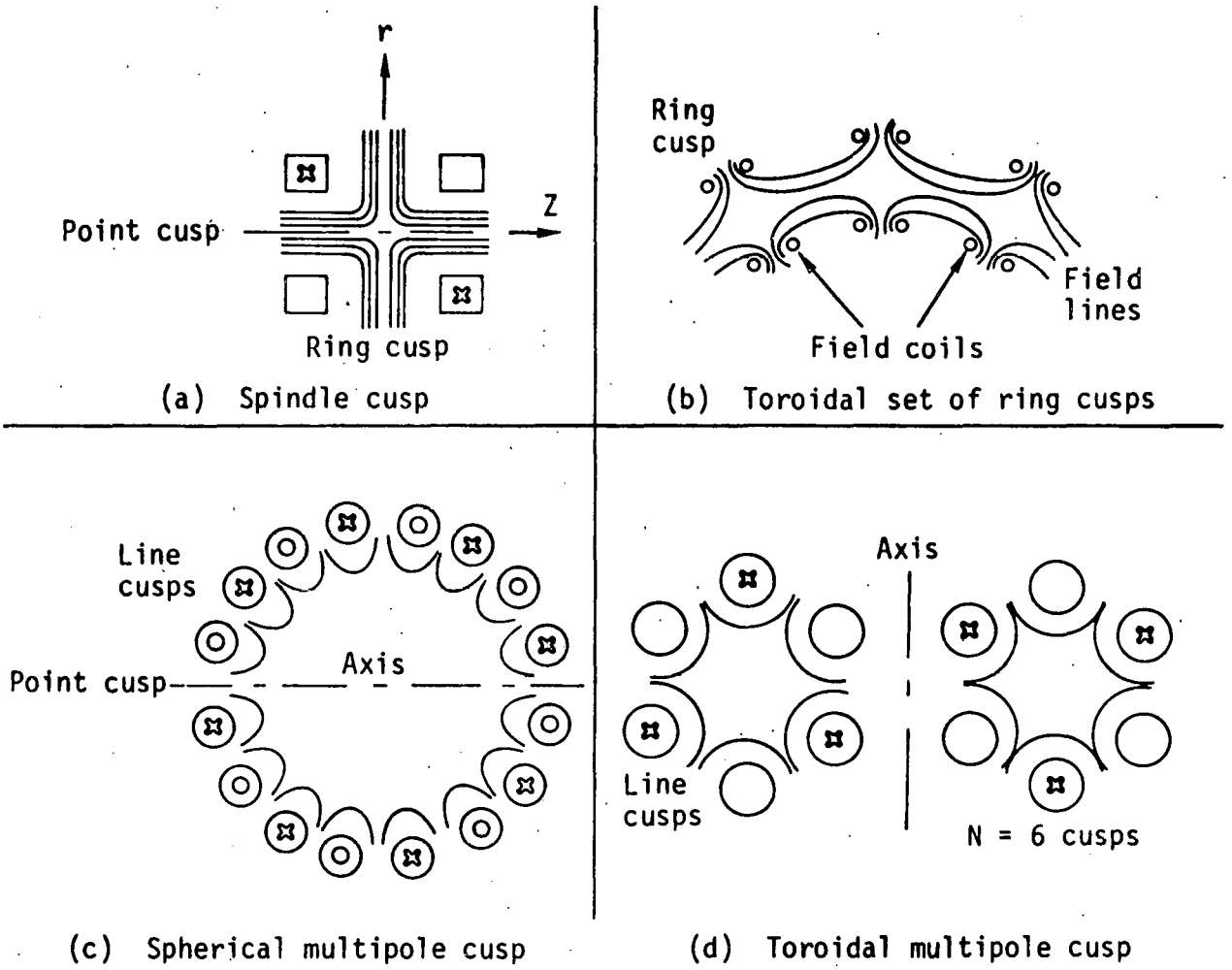

Fig. 15. Some magnetic cusp geometries suitable for electrostatic plugging. (From Ref. 21).

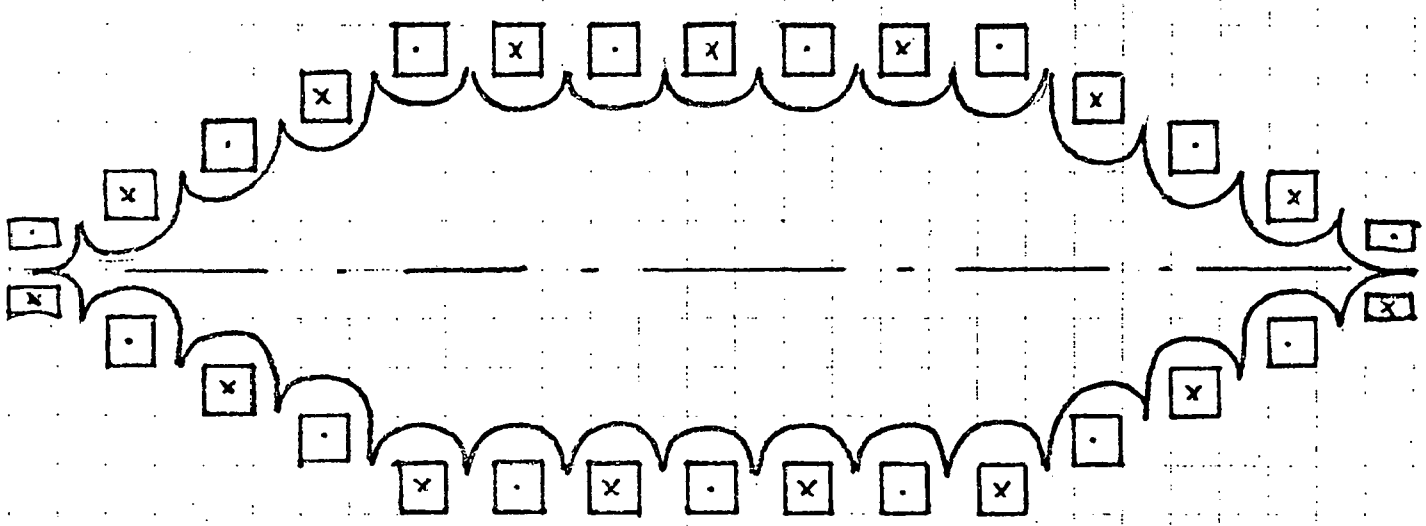

Fig. 16. A linear cusp device composed of many circular coils with alternate current directions.

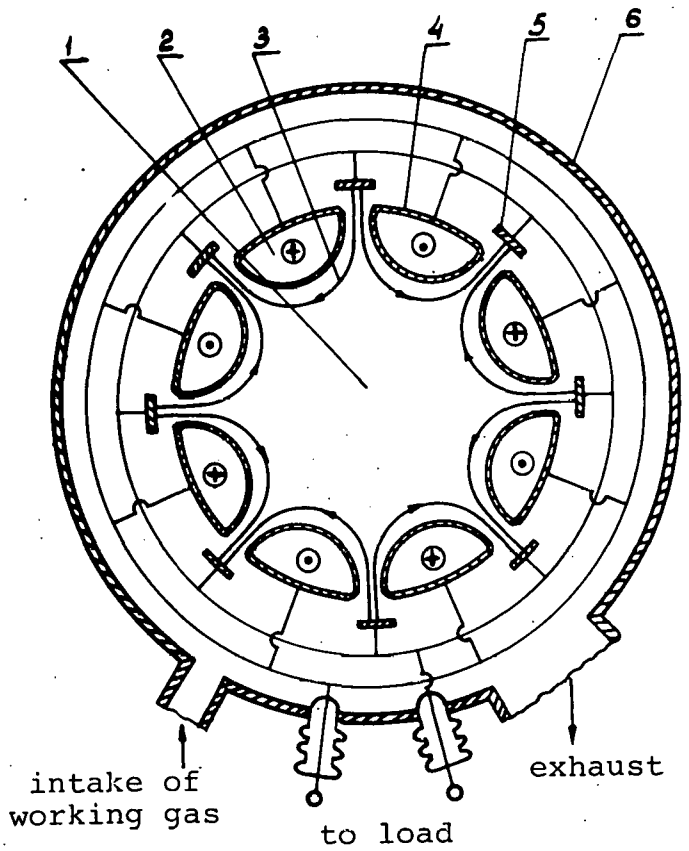

Fig. 17. A spherical electrostatically-plugged cusp fusion reactor scheme.

(1) plasma region
(2) current-carrying conductors (coils)
(3) Magnetic surfaces
(4) wall
(5) plugging electrodes (cathodes)
(6) chamber wall

(from Ref. 36)

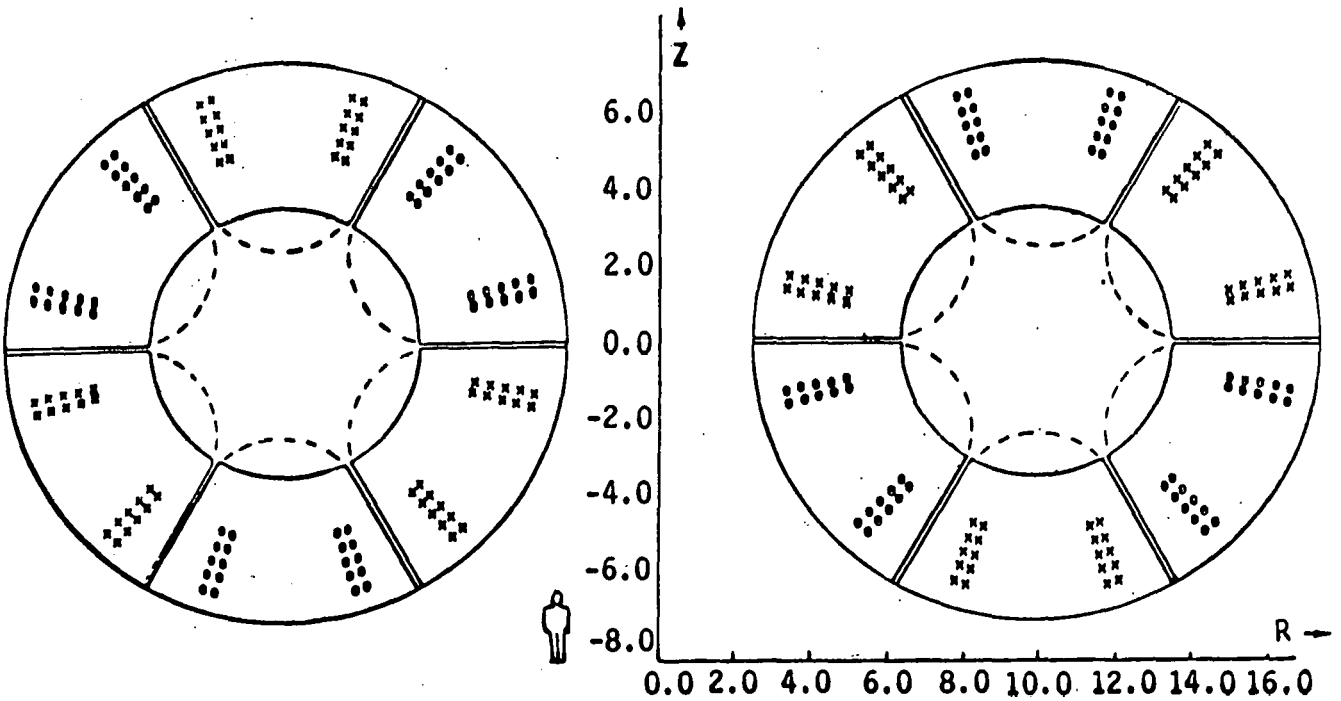

Fig. 18. A large toroidal multipole cusp with N = 6 cusps. (Ref. 21). Dimensions are in meters.

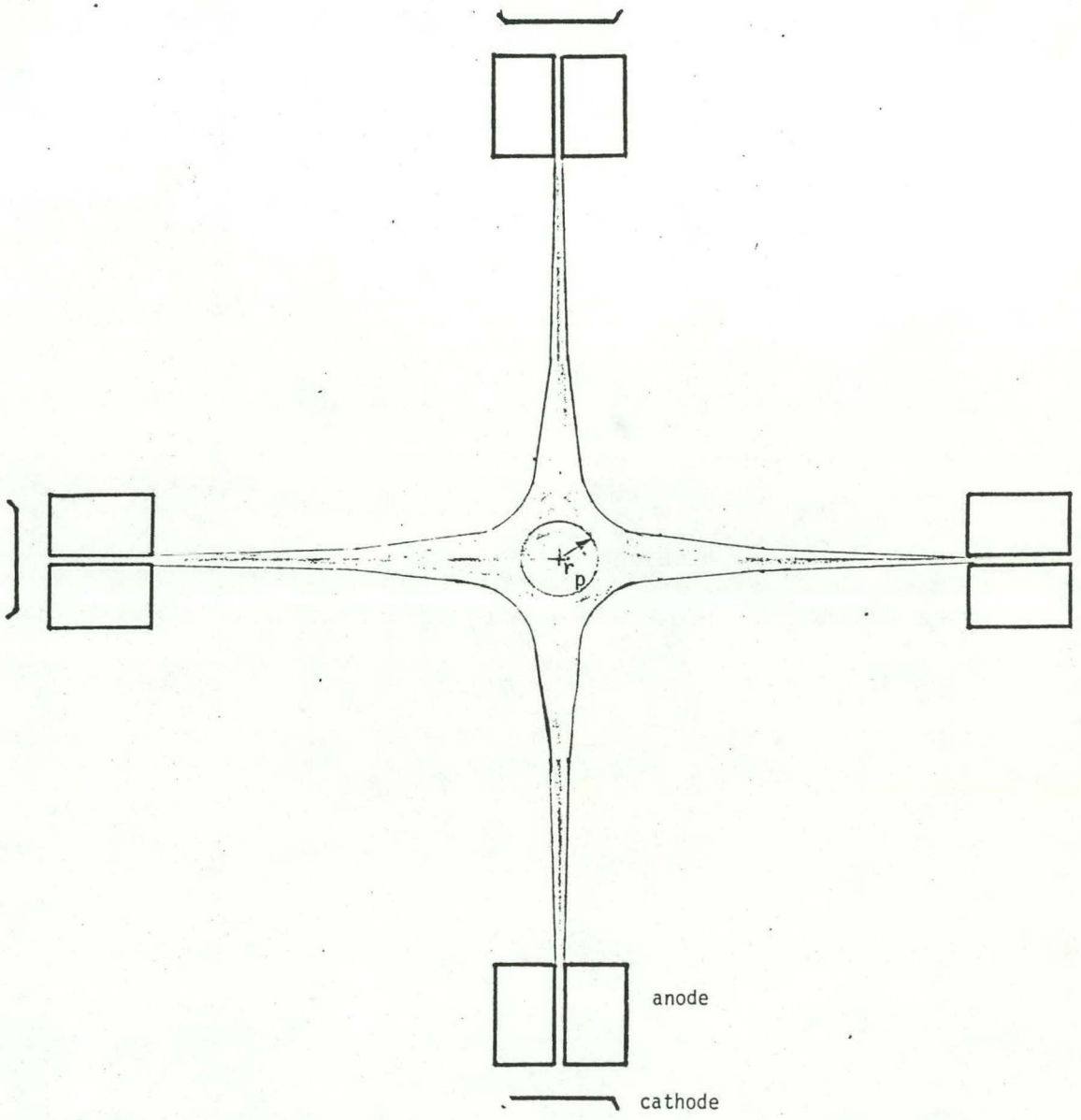

Figure 19a. A small plasma produced by multipoles with N = 4 cusps. Here r_p is the radius to which the plasma excludes the magnetic field.

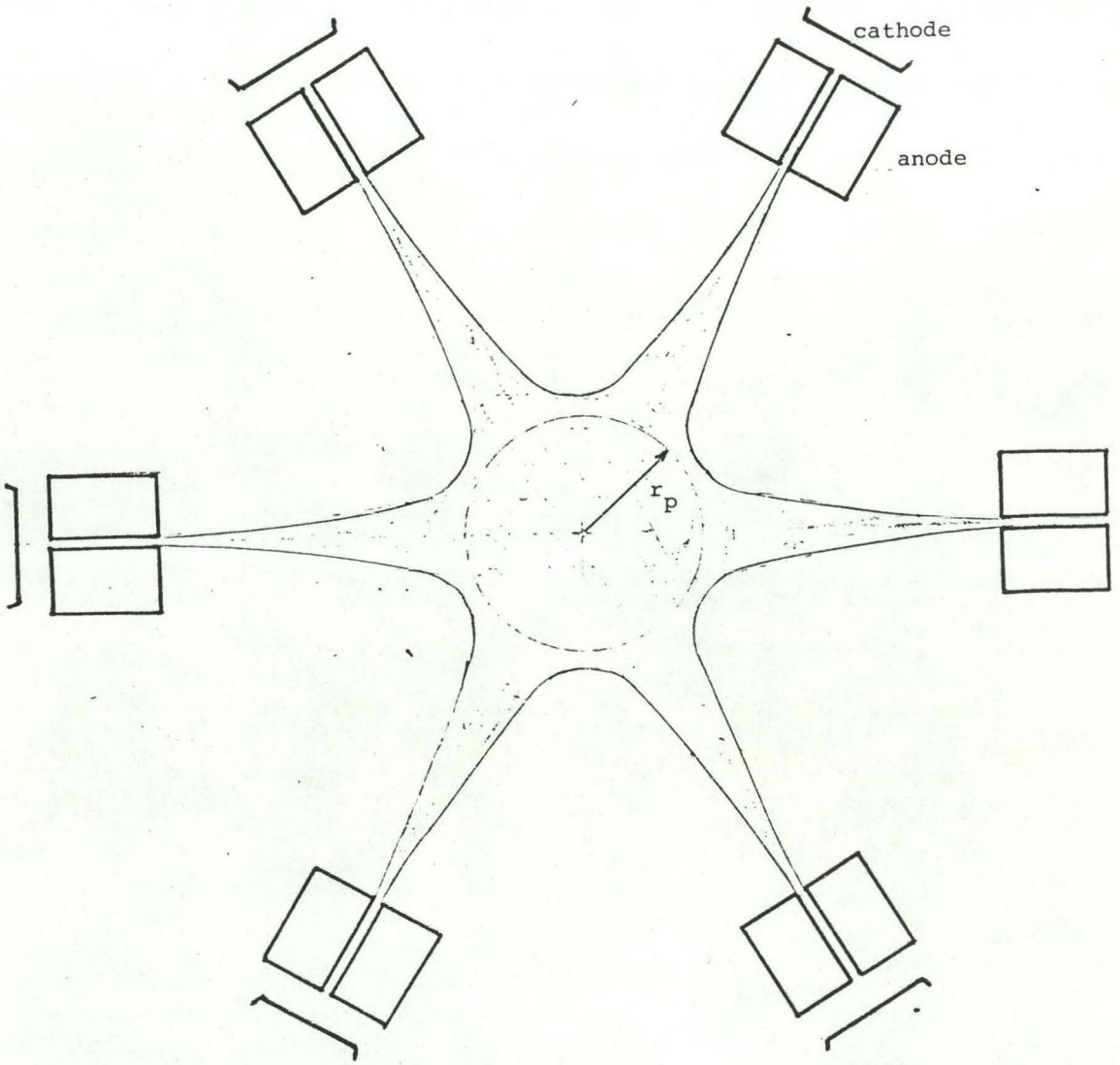

Figure 19b. Same as Fig. 20a, but with N = 6 cusps, hence larger r_p.

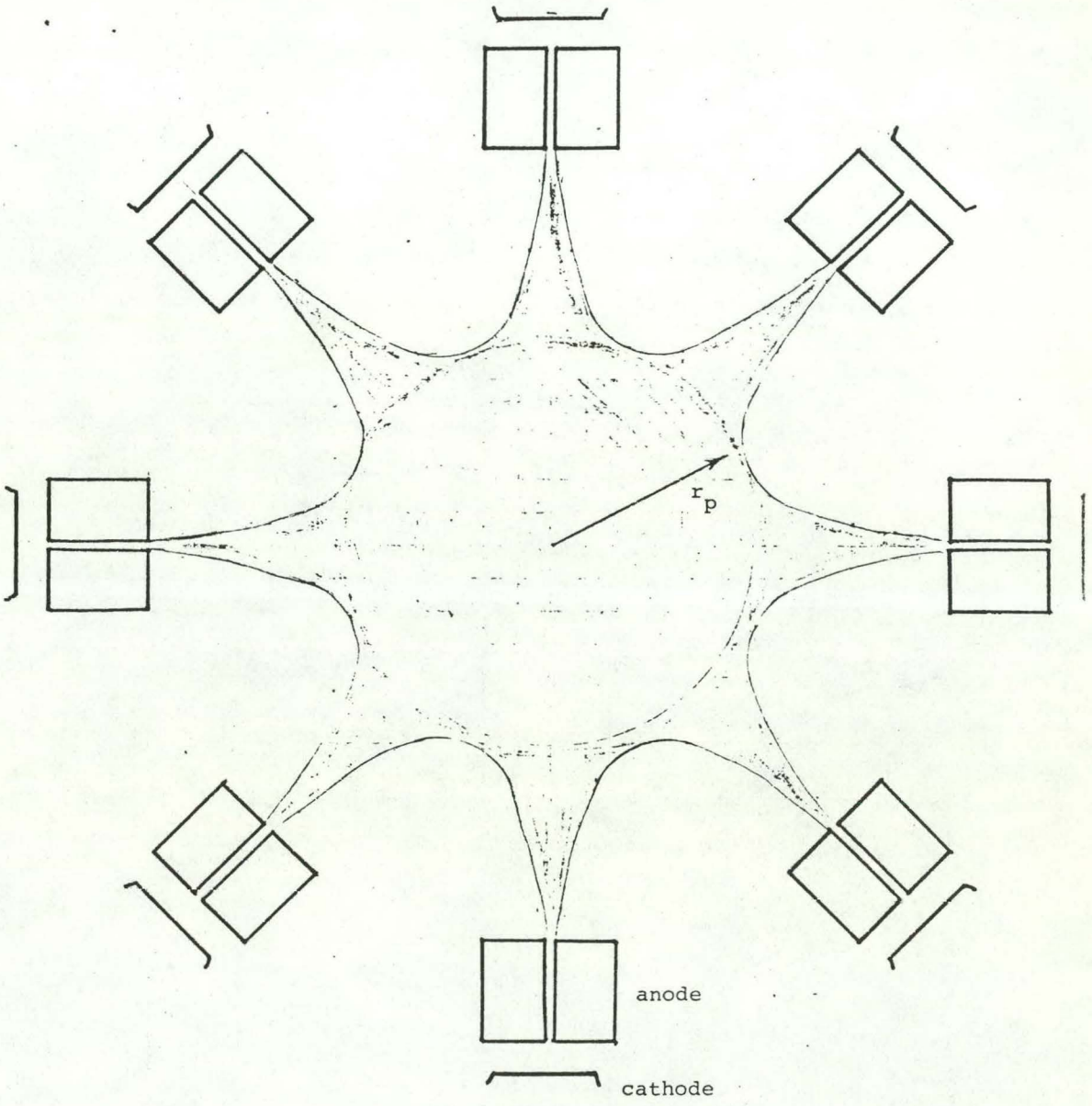

Figure 19c. Same as Fig. 20a, but with N = 8 cusps, and larger r_p.

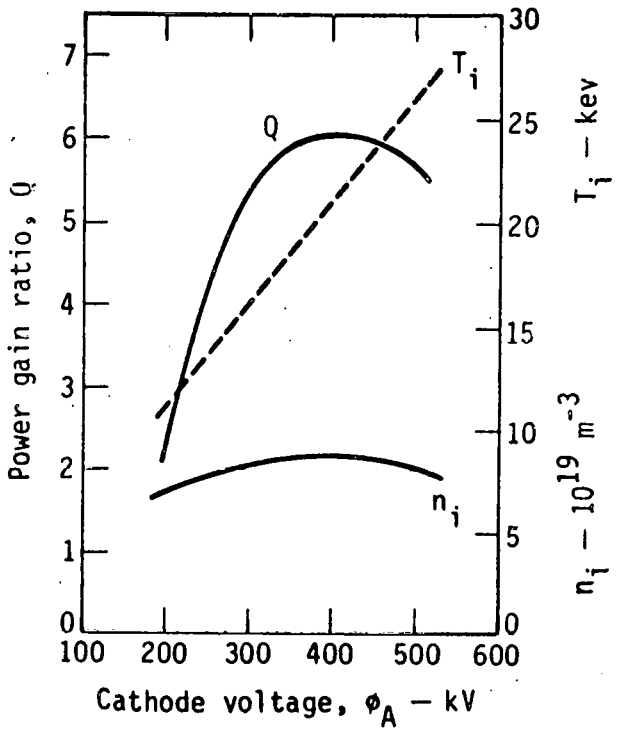

Fig. 20a. Variation of power gain ratio Q, ion density n_i, and ion temperature T_i with applied voltage $_A$, for the case N = 6 cusps (toroidal multipole), B = 8 T, I = 1.0 A/m^3 electron beam injection current, and a 1 % aluminum impurity. (Ref. 21)

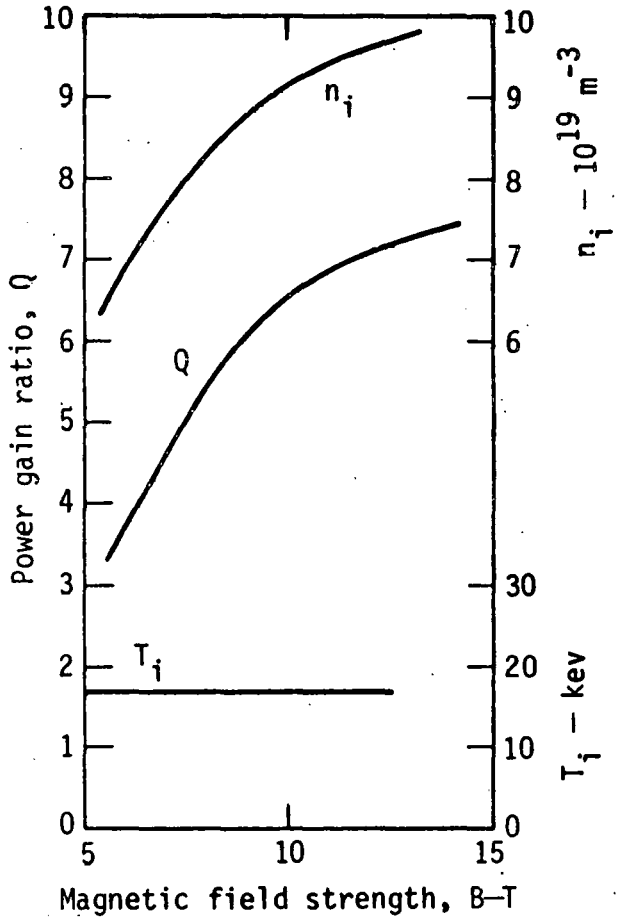

Fig. 20b. Variation of power gain ratio Q, n_i, and T_i with magnetic field B, for ϕ_A = 300 kV and other paramaters the same as the previous Figure. (Ref. 21).

burn lasts 75 sec, and flushing takes 15 sec. One case is for a blanket without beryllium as a neutron multiplier (M = 1.2) and the other cases for a blanket containing beryllium (M = 1.68). (M is the thermal energy deposited in the blanket per neutron incident, divided by 14.1 MeV.) The direct capital costs estimated for this reactor are compared with cost estimates for mirror and Tokamak reactors in Table 4.

Preventing high voltage breakdown is a major problem of electrostatically-plugged fusion devices. One way to avoid breakdown is by using radiation collimators to minimize the radiation incident on the cathodes and to use graduation of the electrostatic potential, as in accelerator design. These techniques are illustrated in Fig. 22. Another major reactor problem is slowing the rate of impurity buildup, which will probably limit fusion burn to about 50-100 sec.

From a physics standpoint, a spherical reactor, such as that of Fig. 17, might provide better plasma parameters than the toroidal multipole of Fig. 18; and from an engineering standpoint, a linear cusp, such as that of Fig. 16, would be cheaper to build and maintain. At present, it appears that point cusps can be at least partially plugged, so that such reactor designs are viable, but the physics of the point cusp plugging is not clearly understood yet.

Table 3. Electrostatically-plugged Toroidal Multipole Cusp Reactor Parameters (Refs. 21, 37)

Coil Configuration	
Toroidal multipole cusp with N = 6 cusps	
Magnetic field in cusp	B = 8 T
Total coil current × length	$= 2.3 \times 10^{10}$ Am
Coil support structure: cryogenic steel trusses supported by fiberglass compression columns and room temperature steel hoops	
Structural steel mass	$= 6 \times 10^{6}$ kg
Vacuum Chamber	
Major radius	R = 10 m
Minor radius	a = 3.6 m
Blanket and shield thickness (assumed)	= 1.5 m
Neutron wall loading	$= 1.6$ MW/m^2
First wall: not designed	
Deuterium-tritium neutral gas feed rate	$I_0 = 2.4 \times 10^{21}$ atoms/s
Electrodes	
Applied voltage	ϕ_A = 300 kV
Cathode current	I = 1.78 kA
Plasma Parameters	
Nominal major radius	R_p = 9.5 m
Nominal minor radius	r_p = 2.8 m
Nominal plasma volume	V = 1470 m^3
Assumed impurity	1% aluminum (Z_{eff} = 2.4)
Electron density	$n_e = 1.0 \times 10^{20}$ m^{-3}

Table 3 Continued

Fuel ion density	$n_i = 8.9 \times 10^{19}$ m^{-3}
Electron temperature	$T_e = 17$ keV
Ion temperature	$T_i = 16.5$ keV
Electron potential barrier	$\phi_e = 88$ kV
Ion potential barrier	$\phi_i = 140$ kV
Potential sag in anodes	$\Delta\phi = 72$ kV
Fusion power density	$P_f/V = 1.89$ MW/m^3
Average electron Larmor radius in cusp	$\rho_e = 6 \times 10^{-5}$ m
Characteristic width of peak of electron density distribution in anodes (assumed)	$2\rho_e$
Boundary layer thickness	10 mm
Debye length in cusp gap	$\lambda_D = 0.2$ mm

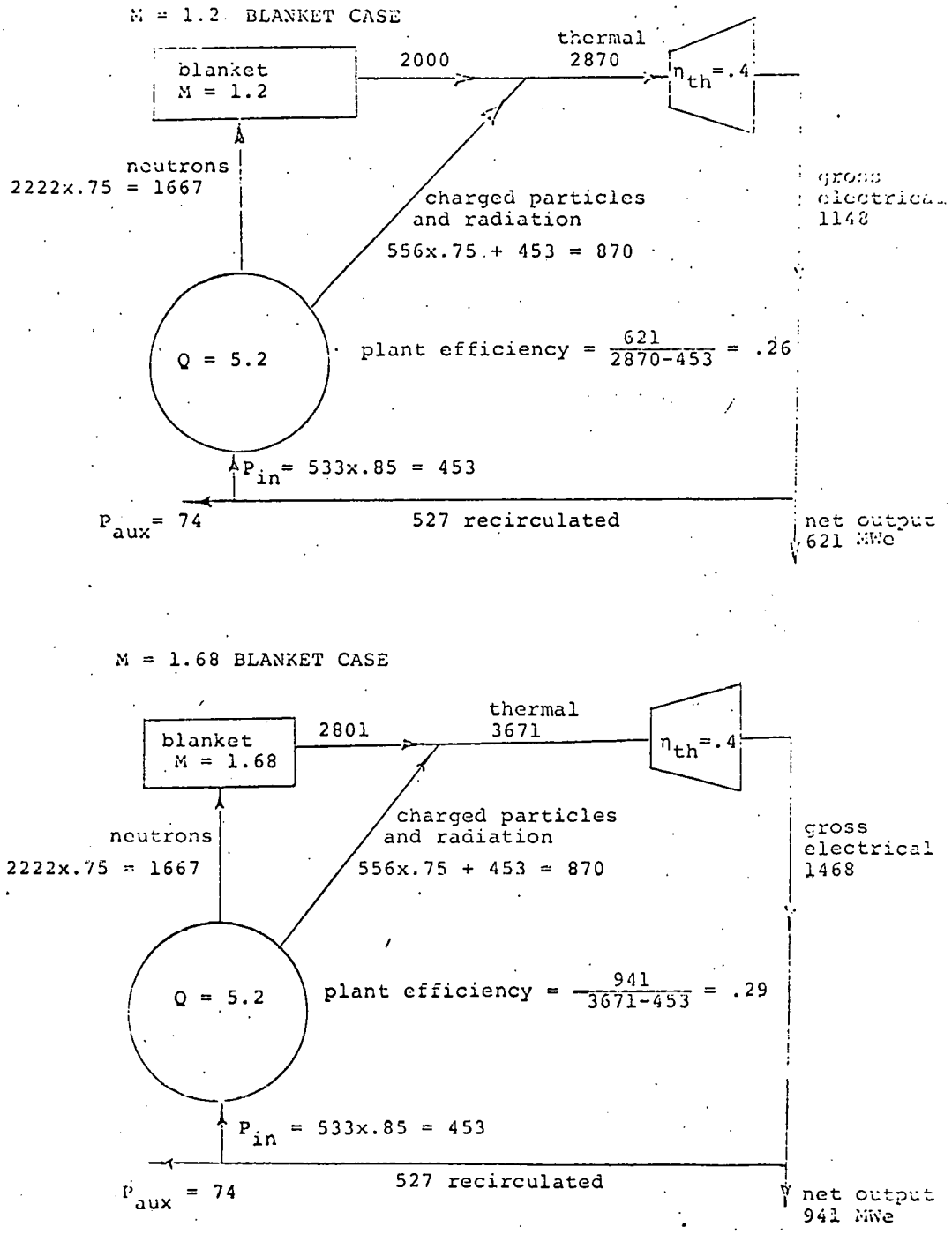

Fig. 21. Power flow diagrams for cusp reactor
Power flows are in MW. (Ref. 37)

Table 4. Comparison of estimated direct capital costs of various fusion reactors, $/kWe. (Ref. 37)

	M = 1.2	M = 1.7
cusp reactor	1400	1000
tandem mirror reactor	1300	-
field reversed mirror reactor	900	700
UWMAK-III Tokamak reactor	1200	

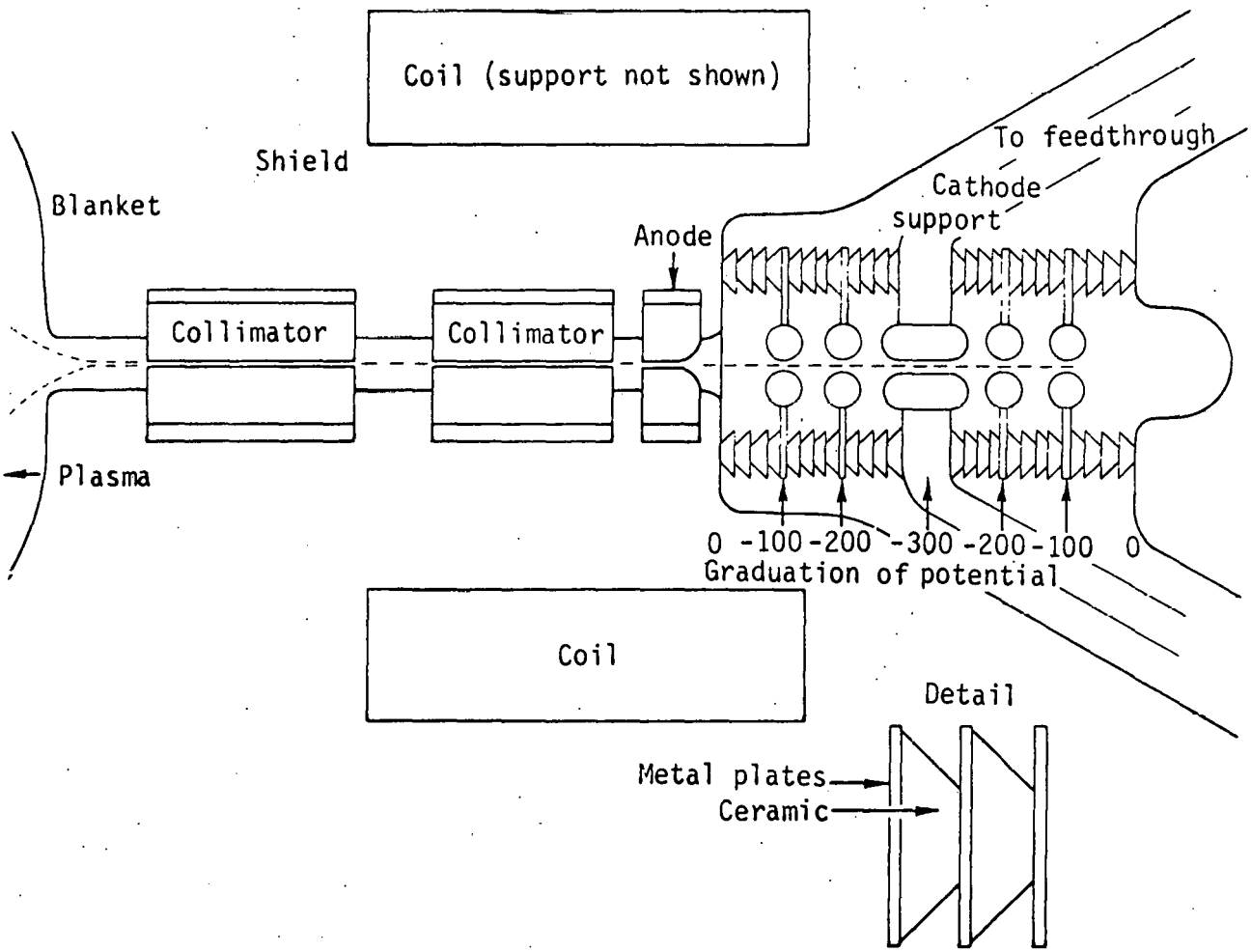

Fig. 22. Reactor coils, electrodes, and radiation collimators. (from Ref. 21)

SIMILARITY OT OTHER PLASMA CONFINEMENT CONCEPTS

In addition to being similar to electrostatic plasma confinement, as discussed previously, electrostatically plugged cusps (EPC) are similar in some ways to Tandem Mirrors, to Tormac, and to SURMAC.

Tandem Mirrors

Fig. 23 shows the axial variations of magnetic field, electron density, and electrostatic potential for a Tandem Mirror plasma confinement system. Intense neutral beam injection in the end "plug" cells (possibly augmented by rf heating) creates a very-high-density plasma there, and leakage from the end cells creates a plasma with a lower density in the low-field solenoid (central cell). The electrostatic potential follows the electron density via the Boltzmann relation

$$\phi(z) = T_e \ln\left(n_e(z)/n_0\right) \tag{30}$$

so electrostatic potential hills with height $\phi_i = T_e \ln\left(n_p/n_e\right)$ are formed by the end plug plasmas.

The potential variation along the magnetic field lines is identical to the potential variation for EPC (Fig. 4), and ion loss parallel to the magnetic field is impeded by the potential barrier ϕ_i. As with electrostatic plugging, the electrons are confined in the parallel direction by the electrostatic potential barrier ϕ_e, and in the perpendicular direction by the magnetic field.

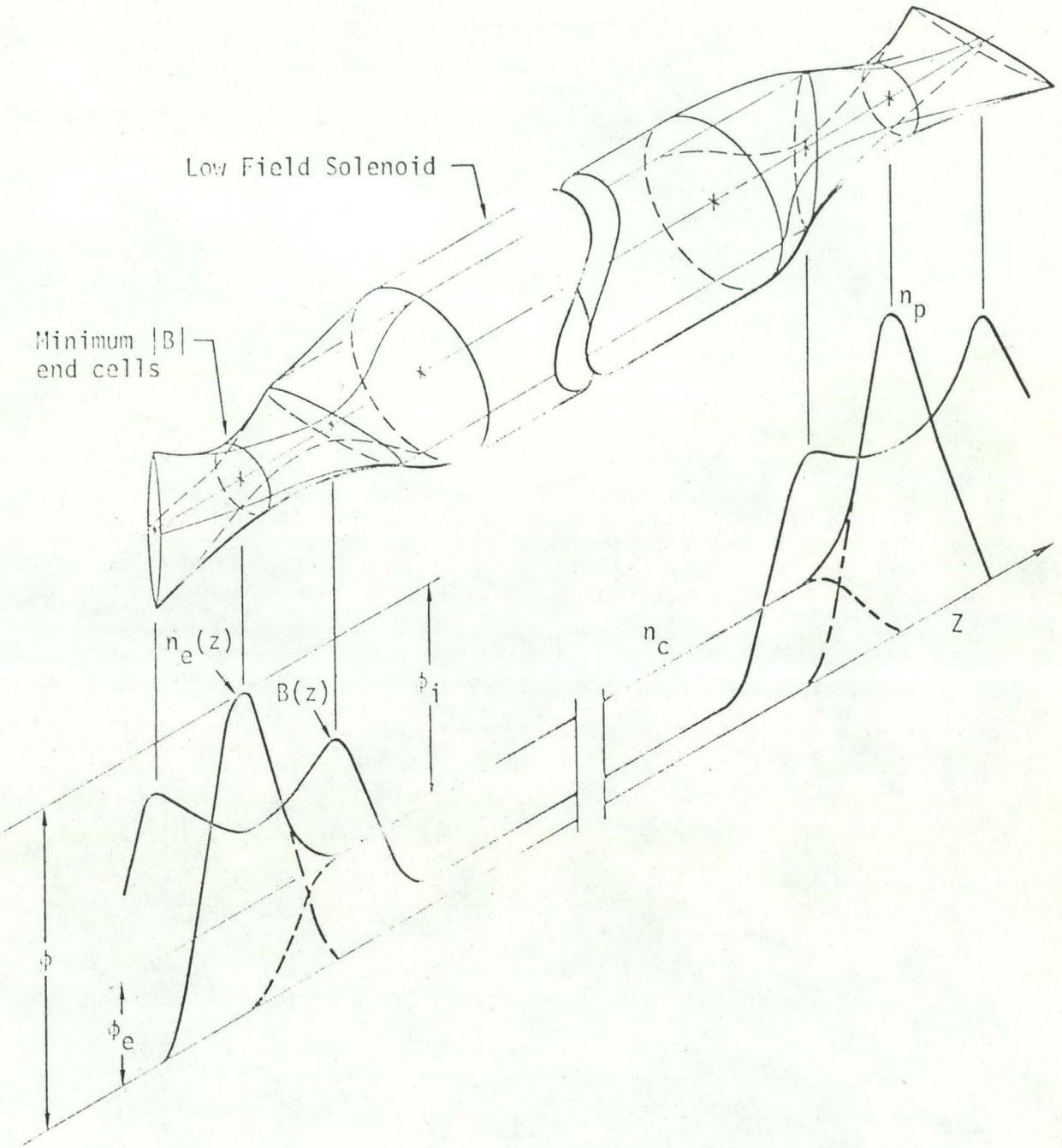

Fig. 23. Axial variations of magnetic field, electron density, and electrostatic potential for the Tandem Mirror plasma confinement system (Ref. 38). The profiles of potential and density have similar shapes.

The main difference between plasma confinement mechanisms in Tandem Mirrors and EPC is that the plasma in Tandem Mirrors is positive relative to the walls, while the plasma in electrostatically plugged cusps is negative relative to the bounding flux surface. This means that ion confinement in the perpendicular direction is magnetic in Tandem Mirrors and electrostatic in EPC. Consequently, fusion product aplhas are poorly confined in EPC and fairly well confined in Tandem Mirrors.

Both devices confine impurities well parallel to the magnetic field, but the Tandem Mirror offers the possibility of expelling impurities via radial diffusion across the magnetic field.

Technologically, Tandem Mirrors require high-efficiency neutral beams at high voltages (~1 MeV), which have not been attained; and EPC require high-voltage electrodes (~300 kV) with close electrode dimensional tolerances.

Tormac

The name "Tormac" stands for "Toroidal Magnetic Cusp." By combining a toroidal cusp magnetic field with a toroidal magnetic field, a plasma confinement geometry is obtained which has closed magnetic flux surfaces on the inside and open field lines on the outside. If a toroidal magnetic field were added to the toroidal cusp of Fig. 15(d), for example, a Tormac configuration would result. An alternative "bi-cusp" Tormac is illustrated in Fig. 24.

Favorable magnetic field gradients and curvature prevent MHD instabilities. The plasma loss from the central region consists

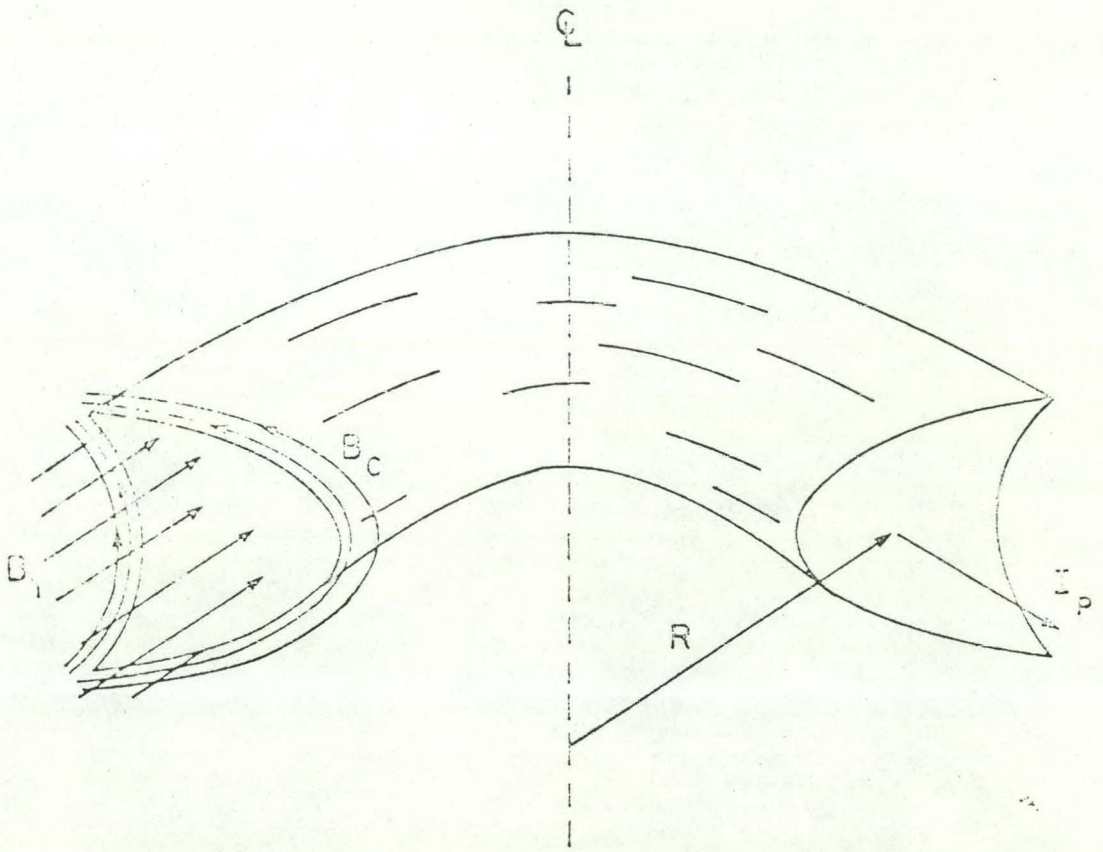

Fig. 24 . The toroidal "bi-cusp" design of TORMAC IV. The plasma is confined by the combination of the cusp field B_c, the toroidal field B_t, and the self-magnetic field of the plasma current I_p. (From Ref. 39).

of two processes in series: diffusion from the central toroidal region into the boundary sheath, followed by mirror-like loss along the open field lines of the sheath region. The rate at which plasma is lost to the walls is

$$nV/\tau \equiv d(nV)/dt \simeq n_s V_s/\tau_{ii} = n_s S\delta/\tau_{ii} \tag{31}$$

where τ is the "confinement time," n and n_s are the plasma densities in the central region and in the sheath, V and V_s are the volumes of the central region and sheath, S is the surface area of the plasma, δ is the sheath thickness, and τ_{ii} is the ion-ion scattering time, which is the effective confinement time for mirror-trapped particles in the sheath. For a cylinder, $V/S = r_p/2$. If the sheath thickness $\delta \simeq 2\rho_i$ (the ion Larmor radius), and if $n_s \simeq n$, then the confinement time is

$$n\tau \simeq n\tau_{ii}\left(r_p/4\rho_i\right) \simeq C_1 r_p B\ T_i \beta^{1/2} \tag{32}$$

where r_p is in meters, B is the external confining magnetic field (T), T_i is the ion temperature (keV), β is the ratio of plasma pressure to $\left(B^2/2\mu_0\right)$, and $C_1 \simeq 4.5 \times 10^{17}\ m^{-4} sec\ T^{-1} keV^{-1}$ (including additional correction factors).[39] Thus, for a typical $\beta \sim 0.7$,

$$n\tau \simeq 4 \times 10^{17} r_p B\ T_i \qquad \left(m^{-3} sec\right). \tag{33}$$

If T_i were replaced by T_e, this equation would be almost identical to Eq. (20) for EPC.

The similarity of the $n\tau$ scalings for Tormac and EPC is a consequence of the fact that both devices have a large-volume central plasma surrounded by a thin surface loss region, in which the loss rate is a function of the number of gyroradii comprising the sheath thickness. For Tormac, the losses are primarily mirror losses along magnetic field lines to the walls at the ion-ion scattering rate; while for EPC the loss is electron diffusion to the walls via momentum-transfer collisions.

Thus, Tormac and EPC have similar magnetic field geometry and confinement time scaling. On the other hand, Tormac does not employ electrostatic confinement of ions; this is a major difference between the two concepts.

Technologically, EPC require high voltage electrodes with close tolerances, while Tormac requires an added toroidal magnetic field. Alpha particle confinement could be enhanced to obtain ignition in EPC by adding such a toroidal magnetic field, at the expense of the added complexity.

SURMAC

The name "SURMAC" stands for "Surface Magnetic Confinement." The SURMAC concept involves surrounding a large-volume, field-free plasma with bumpy magnetic multipole walls. One configuration is illustrated in Fig. 25. This sketch can represent either a long cylinder or a cross section of a torus. If it is a long cylinder, the conductors must be squeezed together at the ends and some form of end-plugging employed (such as electrostatic stoppering). The central plasma region is field-free and uniform, and the magnetic walls shown in the figure provide confinement with good stability against MHD instabilities and microinstabilities, due to favorable magnetic field gradients.

SURMAC configurations are similar to EPC in that both schemes employ some form of high-order multipole field, with a large-volume, field-free plasma surrounded by some sort of magnetic walls having favorable magnetic field gradients. Both have reflection of free electrons by magnetic walls.

SURMAC configurations differ from EPC in that the inner row of SURMAC conductors is completely surrounded by plasma, whereas for EPC the plugging electrodes prevent the plasma from going around behind the coils. Thus, EPC have easy access to the coils for supply of power, shielding, and coolant; while the inner multipole conductors of SURMAC must be suspended either from the ends (of an open-ended device) or by some type of magnetically-shielded support wires (in the case of toroidal SURMAC). Support, shielding, and cooling of the inner row of conductors are major techno-

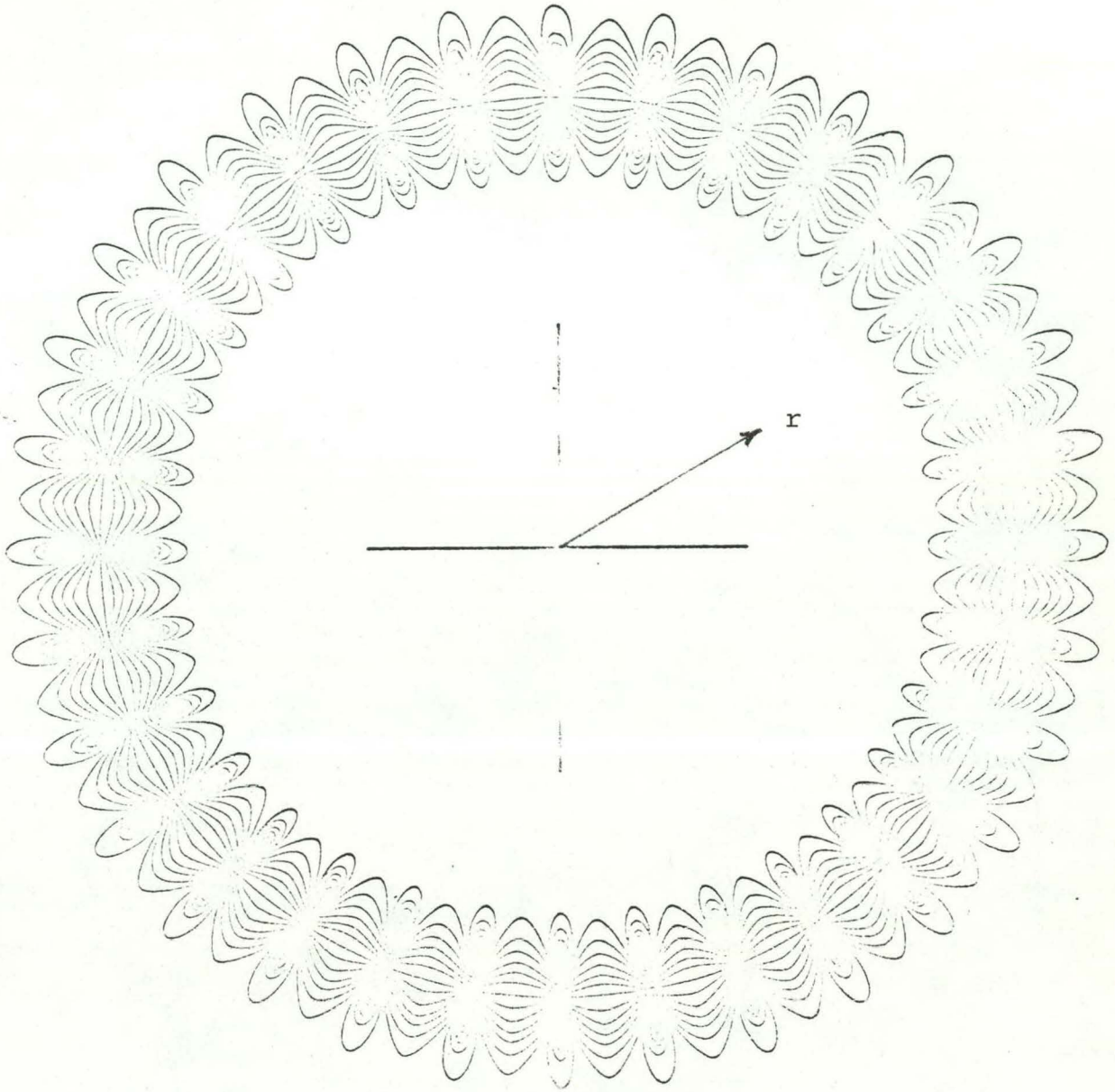

Fig. 25. One type of SURMAC confinement field. This configuration consists of an inner row of conductors with currents in one direction (such as out of the paper) surrounded by an outer row of conductors with currents in the opposite direction (into the paper). This sketch represents the cross section of a long cylinder or torus. (From Ref. 40).

logical problems. Open-ended SURMAC configurations need some form of end-plugging, which could be provided by electrostatic plugs.

Another difference is the thicker plasma in SURMAC between the conductors. The plasma thickness varies from hybrid gyroradii to ion gyroradii, in contrast to the boundary layers of EPC, which are several electron Larmor radii thick.

SUMMARY

Electrostatically plugged cusps offer the following good features:

(1) Plasma in EPC is MHD stable, due to favorable magnetic field gradients.

(2) Plasma in present experiments is stable to long-wave length diocotron modes, due to wall stabilization. Density buildup to the limit imposed by the short-wavelength diocotron mode is observed. The density scales proportional to B^2, which gives densities adequate for a reactor at $B = 7$ T. No other microinstabilities, such as two-stream or drift waves, have been observed, during observation periods lasting many electron-electron scattering times.

(3) Ion temperature is roughly 5-10% of applied voltage.

(4) According to our present concepts of how EPC work, it appears that good values of $n\tau$ (Eq. 20) and Q can be obtained with reasonable values of applied voltage and magnetic field. (However, very little enhancement of transport rates in the boundary layer can be tolerated.) Further experiments are needed to test these concepts.

(5) Since most of the plasma is in a field-free region, and since the electron temperature is not high, cyclotron radiation will be negligible.

(6) Fueling is easy.

(7) A linear reactor with simple geometry is probably feasible (Fig. 16).

(8) Economics estimates for a more complex toroidal multipole EPC reactor design indicate that its direct capital costs are comparable to those of other fusion reactor designs (UWMAK III, Tandem Mirror Reactor).

The following uncertainties exist with regard to EPC:

(1) The theory of the equilibrium boundary layer configuration and transport rates needs to be developed.

(2) A detailed treatment of plasma stability in the boundary layer needs to be developed. (Stability of the central large-volume plasma is assured by its being homogeneous and free of electric or magnetic fields).

(3) Uncertainties of plasma parameter variations need to be resolved by comprehensive diagnostic measurements, especially in the boundary layer, at higher values of τ_{Ee}/τ_{ee}, approaching the reactor regime.

(4) Technological uncertainties of electrode alignment, voltage holding, and impurity buildup rates need to be decided by experimental research.

In conclusion, electrostatically plugged cusp experiments have produced interesting plasma parameters, in some cases better than expected, but much more research is needed before we will be able to say that we understand what is going on.

ACKNOWLEDGEMENTS

The author is grateful to R. W. Moir and W. L. Barr for helpful discussions, and to B. C. Gregory, B. L. Stansfield, J. M. Larsen, and J. P. Matte for information on their recent progress.

REFERENCES

1. O. A. Lavrent'ev, "On Electrostatic Plasma Confinement I," Ukrayin. Fiz. Zh. 8, 440 (1963) (In Ukrainian).
2. W. C. Elmore, J. L. Tuck, and K. M. Watson, "On the Inertial Electrostatic Confinement of a Plasma," Phys. Fluids 2, 239 (1959).
3. O. A. Lavrent'ev, "Investigation of an Electromagnetic Trap," Magnitnye lovushki, Vypusk 3, Naukova Dumka, Kiev, USSR (1968). Translation: AEC-tr-7002 (Rev).
4. R. L. Hirsch, "Inertial-electrostatic Confinement of Ionized Fusion Gases," J. Appl. Phys. 38, 4522 (1967).
5. B. E. Cherrington, J. T. Verdeyen and D. A. Swanson, "Recent Developments in Electrostatic Confinement--Theoretical," Ann. N. Y. Acad. Sci. 251, 139 (1975).
6. J. T. Verdeyen, B. E. Cherrington, D. A. Swanson, and D. J. Meeker, "Recent Developments in Electrostatic Confinement--Experimental," Ann. N. Y. Acad. Sci. 251, 126 (1975).
7. O. A. Lavrent'ev, L. I. Ovcharenko, B. G. Safronov, and V. A. Sidorkin, "Electron Injection into an Electromagnetic Trap," Ukrayin. Fiz. Zh. 11, 982 (1966) (In Ukrainian).
8. N. Hershkowitz and J. M. Dawson, "Fusion Reactor with Picket Fence Walls," Nucl. Fusion 16, 639 (1976).
9. R. W. Moir, "A New Magnetic Well Configuration, Importance of the Mirror Ratio, and Electrostatic Containment of Warm Plasma," EUR-CEA-FC-496, Fontenay-aux-Roses, France (1968).

10. J. L. Hilton, C. K. Hinrichs, and A. A. Ware, "Theoretical and Experimental Results on the Electrostatic Plugging of a Cusp Containment System," Plasma Phys. 10, 455 (1968).

11. A. A. Ware and J. E. Faulkner, "Electrostatic Plugging of Open-Ended Magnetic Containment Systems," Nucl. Fusion 9, 353 (1969).

12. W. Strijland, "Diffusion of Electrons in a Magnetic Bottle of Cusped Geometry," Physica 47, 617 (1970).

13. O. A. Lavrent'ev, "Electrostatic and Electromagnetic High-temperature Plasma Traps," Ann. N. Y. Acad. Sci. 251, 152 (1975).

14. G. I. Budker, "Thermonuclear Reactions in a Potential Well of a Negative Charge," Plasma Physics and the Problem of Controlled Thermonuclear Reactions, Vol. I (translation by Pergamon Press, N. Y., 1961), p. 295.

15. T. H. Stix, "Ion Containment Sources," IEEE Trans. Nucl. Sci. NS-19, 150 (1972).

16. V. L. Sizonenko and K. N. Stepanov, "Electron Confinement in an Electromagnetic Trap," Sov. Phys. Tech. Phys. 20, 468 (1976).

17. V. P. Pastukhov, "Collisional Losses of Electrons from an Adiabatic Trap in a Plasma with a Positive Potential." Nucl. Fusion 14, 3 (1974).

18. V. A. Sidorkin and O. A. Lavrent'ev, "Critical Loss Angles in a Multipole Electromagnetic Trap," Plasma Physics and the Problem of Controlled Thermonuclear Fusion, Vol. 2, Acad. Sci. of the Ukrainian SSR, Naukova Dumka, Kiev (1971), p. 247. (in Russian).

19. R. W. Moir, W. L. Barr, and R. F. Post, "Experimental Results on Electrostatic Stoppering," Phys. Fluids 14, 2531 (1971).

20. Yu. A. Pankrat'ev, V. A. Naboka, S. A. Vlovin, O. A. Lavrent'ev, and A. A. Kalmykov, "Accumulation and Confinement of Plasma in Electromagnetic Traps," Voprosi Atomnoi Nauki i Tekhniki--Ser. Fiziki Plazmy i Problemy Upravlyaemykh Termoyadernykh Reaktsii, No. 1 (3), Fiz.-Tekh. Inst. AN USSR, Khar'kov (1975). Translation: UCRL-Trans-11142 (1976).

21. T. J. Dolan, "Design Study of Electrostatically Plugged Cusp Fusion Reactor," UCRL-52142 (1976).

22. K. D. Marx, T. J. Dolan, R. W. Moir, and C. E. McDowell, "Trapping Rates and Loss Rates for Electrons in an Electrostatically Plugged Cusp," Bull. Am. Phys. Soc. 21. 1044 (1976).

23. J. L. Carter and E. D. Cashwell, Particle-Transport Simulation with the Monte Carlo Method, TID-26607, Tech. Info. Center, U. S. ERDA, Oak Ridge, TN, 1975.

24. R. W. Moir, Personal Communication, 1977.

25. D. J. Rose and M. Clark, Jr., Plasmas and Controlled Fusion, The MIT Press, Cambridge, MA, 1961.

26. R. L. Hayward and T. J. Dolan, "Plasma Density in an Electrostatically Plugged Spindle Cusp," Phys. Fluids 20, 646 (1977).

27. T. J. Dolan, J. M. Larsen, and B. L. Stansfield, "Theoretical Confinement Times in Electromagnetic Traps," Can. J. Phys. 53, 2341 (1975).

28. O. Buneman, R. H. Levy, and L. Linson, "Cross-field Electron Beam Stability," J. Appl. Phys. 37, 3203 (1966).

29. D. G. Blondin and T. J. Dolan, "Equilibrium Plasma Conditions in Electrostatically Plugged Cusps and Mirrors," J. Appl. Phys. 47, 2903 (1976).

30. B. L. Stansfield, Personal Communication, 1977.

31. V. I. Tereshin, "The Results of Plasma Accumulation and Confinement Investigation in KhPTI Pulsed Electromagnetic Traps," presented at the LLL Q-Enhancement Workshop, Sept., 1976.

32. B. L. Stansfield, J. M. Larsen, B. Bergevin, P. Couture, and B. C. Gregory, "Density and Lifetime Measurements in the KEMP II Electromagnetic Trap," Can. J. Phys. 54, 1856 (1976).

33. R. W. Moir, T. J. Dolan, and W. L. Barr, "Design of Electrostatic End-plugged Plasma Confinement Device," to be published in Proc. Symposium on Eng. Problems of Controlled Thermonuclear Research, Knoxville, TN (IEEE, 1977).

34. T. J. Dolan, B. L. Stansfield, and J. M. Larsen, "Plasma Potential in Electrostatically Plugged Cusps and Mirrors," Phys. Fluids 18, 1383 (1975).

35. Yu. I. Pankrat'ev, V. A. Naboka, E. F. Ponomarenko, and O. A. Lavrent'ev, "Crossed-field Plasma Discharges at Low Pressures," Nucl. Fusion 12, 391 (1972).

36. O. A. Lavrent'ev, A. A. Kalmykov, A. V. Georgiyevskiy, V. Ye. Ziser, and V. B. Yuferov, "The 'Jupiter' Thermonuclear Reactor Based on Confinement of Plasma by Electrical and

Magnetic Fields," No. 12 in the series: Sistemnyy Analiz i Konstruktsii Termoyadernykh Stantsiy (Systems Analysis and Design of Thermonuclear Stations). Paper delivered at a joint USSR-USA seminar, December, 1974.

37. T. J. Dolan, "Cost Estimate for Electrostatically Plugged Cusp Reactor," Lawrence Livermore Laboratory report in preparation.

38. F. H. Coensgen, "TMX Major Project Proposal," LLL-Prop-148 (1977).

39. W. B. Kunkel, I. G. Brown, and M. A. Levine, "Scaling for TORMAC Fusion Reactors," Bull. Am. Phys. Soc. 21, 1063 (Nov. 1976).

40. A. Y. Wong, "Surface Magnetic Confinement--a Review," Report PPG-235, Univ. of Cal. at Los Angeles, 1976.

Printed in the United States of America
Available from
National Technical Information Service
U.S. Department of Commerce
5285 Port Royal Road
Springfield, VA 22161
Price: Printed Copy $: Microfiche $3.00

Page Range	Domestic Price	Page Range	Domestic Price
001–025	$ 3.50	326–350	10.00
026–050	4.00	351–375	10.50
051–075	4.50	376–400	10.75
076–100	5.00	401–425	11.00
101–125	5.50	426–450	11.75
126–150	6.00	451–475	12.00
151–175	6.75	476–500	12.50
176–200	7.50	501–525	12.75
201–225	7.75	526–550	13.00
226–250	8.00	551–575	13.50
251–275	9.00	576–600	13.75
276–300	9.25	601–up	*
301–325	9.75		

*Add $2.50 for each additional 100 page increment from 601 to 1,000 pages; add $4.50 for each additional 100 page increment over 1,000 pages.

Technical Information Department
LAWRENCE LIVERMORE LABORATORY
University of California | Livermore, California | 94550